iScience

CellPress
OPEN ACCESS

Article

Single-cell transcriptomics reveals the role of antigen presentation in liver metastatic breast cancer

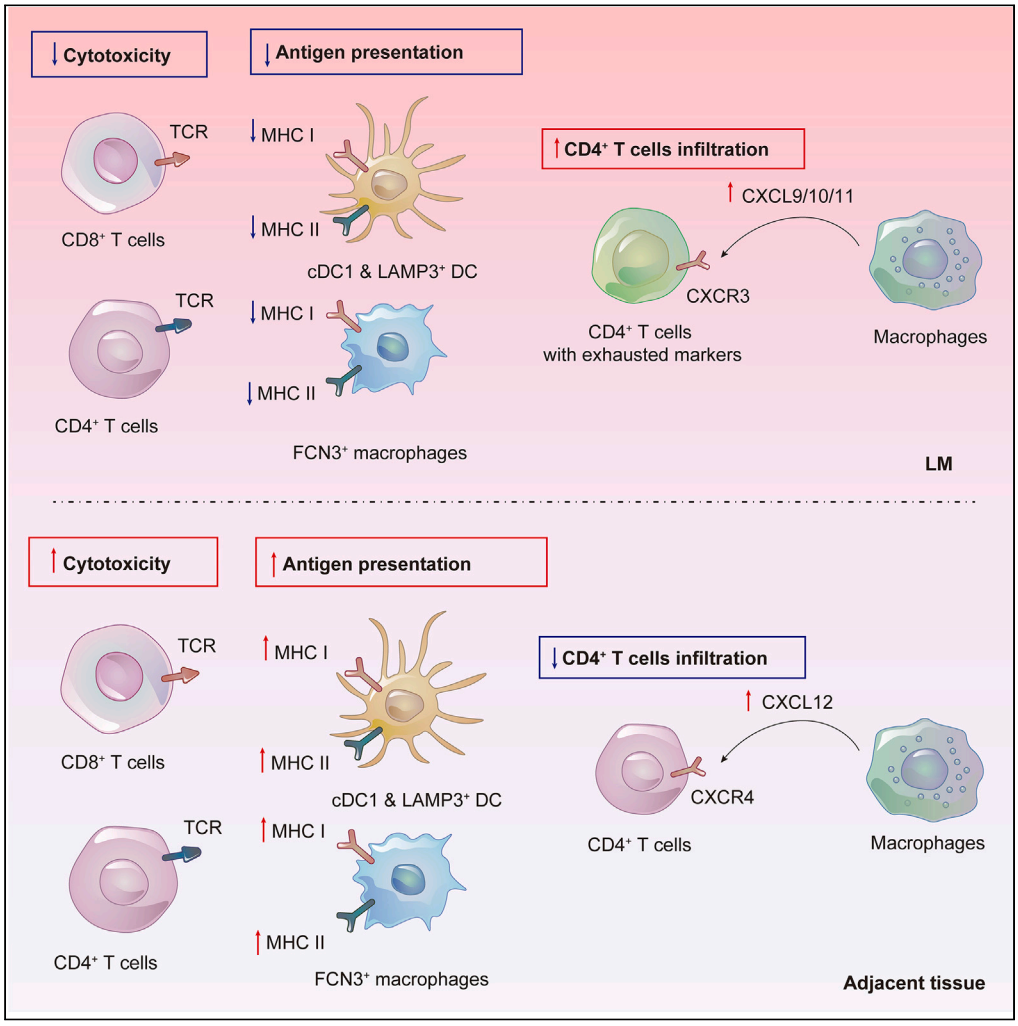

Xiaoshuang Wang, Yan Zhou, Zhongen Wu, ..., Di Zhu, Ming-Wei Wang, Lu Wang

zhudifudan@163.com (D.Z.)
mwwang@simm.ac.cn (M.-W.W.)
cms024mm@163.com (L.W.)

Highlights

ScRNA-seq analysis reports key immune cells and their function in the TME of BC-LM

Exhausted CD4$^+$ and dysfunctional CD8$^+$ T cells were enriched in metastatic tumor

FCN3$^+$ macrophages, cDC1 and LAMP3$^+$ DC regulate T cell functions probably via APP

More MHC$^+$ in the above cells display in LM than in normal tissues and primary BC tumor

Wang et al., iScience 27, 108896
February 16, 2024
https://doi.org/10.1016/j.isci.2024.108896

iScience

CellPress
OPEN ACCESS

Article

Single-cell transcriptomics reveals the role of antigen presentation in liver metastatic breast cancer

Xiaoshuang Wang,[1,7] Yan Zhou,[2,7] Zhongen Wu,[3,7] Cao Xie,[4] Weiqi Xu,[1] Qingtong Zhou,[3] Dehua Yang,[2] Di Zhu,[3,5,*] Ming-Wei Wang,[3,6,8,*] and Lu Wang[1,*]

SUMMARY

Liver metastasis (LM) is the primary cause of cancer-related mortality in late-stage breast cancer (BC) patients. Here we report an in-depth analysis of the transcriptional landscape of LM of 11 patients with secondary hepatic carcinoma at single-cell resolution. Our study reveals that terminally exhausted CD4$^+$ and dysfunctional CD8$^+$ T cells were enriched in LM along with low antigen presentation. We also found that macrophages were associated with the tumor infiltrating CD4$^+$ T cells, while FCN3$^+$ macrophages, type 1 conventional dendritic cells (cDC1) and LAMP3$^+$ DC regulated T cell functions, probably via antigen processing and presentation. Major histocompatibility complex expression in FCN3$^+$ macrophage, cDC1 and LAMP3$^+$ DC was reduced in LM compared to those in normal tissues and primary BC. Malfunctioned antigen presentation in these cells is linked to a worse prognosis in invasive BC and hepatocellular carcinoma. Our results provide valuable insights into the role of tumor infiltrating T cells in LM.

INTRODUCTION

Liver is one of the most common metastatic organs in cancer. Up to 50% of cancer patients have liver metastasis (LM),[1] but their responses to immunotherapy were usually lower than those without it.[2–4] Metastatic liver cancer is a general term for metastases of other malignant tumors initially transferred to the liver and is also referred to as secondary hepatocarcinoma. Due to different sources of primary tumors, LM is highly heterogeneous. In addition, the unique liver structure, such as stellate cells, sinusoidal endothelial cells, and the microenvironment may be susceptible to host metastatic tumors.[5,6] However, the underlying mechanisms remain unclear.

The microenvironment of LM is intricately composed. Unlike other tissues, in which T cell activation usually leads to immune tolerance or anergic hepatic lymphocytes, the liver contains a variety of antigen-presenting cells (APC), including resident liver macrophages called Kupffer cells (KCs),[7,8] liver sinusoidal endothelial cells (LSECs),[9,10] and hepatic stellate cells (HSCs).[11,12] They not only promote T cell tolerance but also participate in the microenvironment suitable for LM. In this regard, single-cell RNA sequencing (scRNA-seq) technology may allow us to systematically analyze the cellular landscape of the microenvironment of LM originated from different organs (Table 1).

In this study, we report the results of 11 scRNA-seq analyses collected from 11 patients with LM (Figure 1A) and took 6 cases of breast cancer (BC) as an example to explore potential mechanisms related to tumor cell seeding. Then, we explored two cases of nasopharyngeal carcinoma (NPC), two cases of thyroid carcinoma (THCA), and one case of cervical carcinoma (CESC) to see if mechanisms found in BC were also shown in other cancers. Combined with the existing *in situ* cancer pathology database, we are able to establish a preliminary microenvironment landscape of pan-cancerous LM, thereby laying a foundation of mechanistic elucidation and response prediction.

RESULTS

Molecular characteristics of LM from BC

LM was found in approximately 50% of patients with metastatic BC.[13] We first investigated the transcriptional and cellular landscape of tumor microenvironment (TME) of 6 female BC patients aged between 44 and 62 following surgical resection of liver metastatic lesions. They were

[1]Fudan University Shanghai Cancer Center, Shanghai Medical College, Fudan University, Shanghai 200032, China
[2]The National Center for Drug Screening and the State Key Laboratory of Chemical Biology, Shanghai Institute of Materia Medica, Chinese Academy of Sciences (CAS), Shanghai 201203, China
[3]School of Basic Medical Sciences, Fudan University, Shanghai 200032, China
[4]School of Pharmacy, Fudan University, Shanghai 201203, China
[5]Minhang Hospital and Shanghai Medical College, Fudan University, Shanghai 201100, China
[6]Research Center for Deepsea Bioresources, Sanya, Hainan 572025, China
[7]These authors contributed equally
[8]Lead contact
*Correspondence: zhudifudan@163.com (D.Z.), mwwang@simm.ac.cn (M.-W.W.), cms024mm@163.com (L.W.)
https://doi.org/10.1016/j.isci.2024.108896

Table 1. Overview of using scRNA technology to study cancer liver metastasis

Year	Tumor type	DOI	Technology used	Species of research objects	Research conclusion
2017	Small-cell lung cancer	https://doi.org/10.1093/annonc/mdx182	Single cell whole genome sequencing	One human patient	1. In this SCLC patient the liver-metastasis founder cells were present in the primary tumor as a minor clone. 2. Close association of the liver metastasis cells, which supports the low intra - tumor heterogeneity in liver metastasis. 3. In this patient, the lymph node and adrenal metastases were spread by polyclonal and liver metastasis by monoclonal.
2020	Lung cancer	https://doi.org/10.1016/j.ccell.2020.06.012	Single-cell RNA sequencing single-cell ATAC-Seq	Genetically engineered mouse models; PDX mice models	1. Lung cancer progression is accompanied by a stereotypic expansion of heterogeneity. 2. Cell state heterogeneity arises largely independently of genetic variation. 3. State transitions occur via an high-plasticity cell state harboring high differentiation and growth capacity. 4. The high-plasticity cell state is drug resistant and portends poor patient survival across all cancers.
2021	Gallbladder cancer	https://www.ncbi.nlm.nih.gov/pmc/articles/PMC8184464/	Single-cell RNA sequencing	One human patient	1. Malignant cells displayed a high degree of intratumor heterogenicity. 2. Neutrophils were found to promote GBC cell proliferation, migration, and invasion. 3. Cytotoxic cluster of differentiation ($CD8^+$) T cells became exhausted and $CD4^+$ regulatory T cells (Tregs) exhibited immunosuppressive characteristics. 4. Cancer-associated fibroblasts exhibited heterogeneity and may be associated with GBC metastasis.
2021	Pancreatic cancer	https://doi.org/10.1016/j.celrep.2021.108990	Single-cell RNA-sequencing	Genetically engineered mouse models	1. Single-cell RNA-seq reveals a continuum of cancer epithelial-mesenchymal transition. 2. Genetic deletion of both Snai1 and Twist1 or Zeb1 stabilizes epithelial phenotypes. 3. Epithelial cancer cells have increased liver metastasis and collectively migrate. 4. Mesenchymal-like cancer cells recruit fewer T cells.

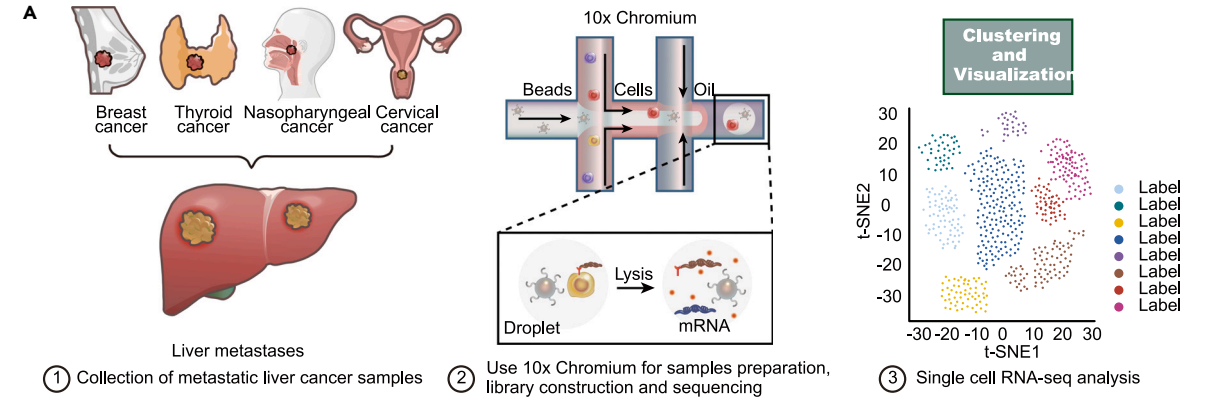
A
Breast cancer
Thyroid cancer
Nasopharyngeal cancer
Cervical cancer
Liver metastases
1 Collection of metastatic liver cancer samples
10x Chromium
Beads
Cells
Oil
Lysis
Droplet
mRNA
2 Use 10x Chromium for samples preparation, library construction and sequencing
Clustering and Visualization
t-SNE2
t-SNE1
Label
3 Single cell RNA-seq analysis

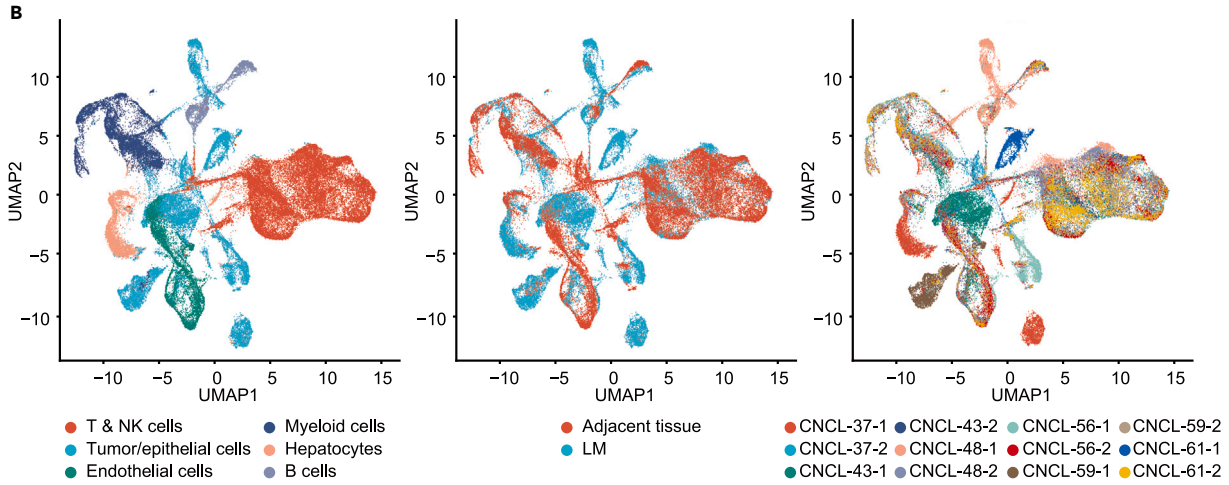
B
UMAP2
UMAP1
T & NK cells
Tumor/epithelial cells
Endothelial cells
Myeloid cells
Hepatocytes
B cells
Adjacent tissue
LM
CNCL-37-1
CNCL-37-2
CNCL-43-1
CNCL-43-2
CNCL-48-1
CNCL-48-2
CNCL-56-1
CNCL-56-2
CNCL-59-1
CNCL-59-2
CNCL-61-1
CNCL-61-2

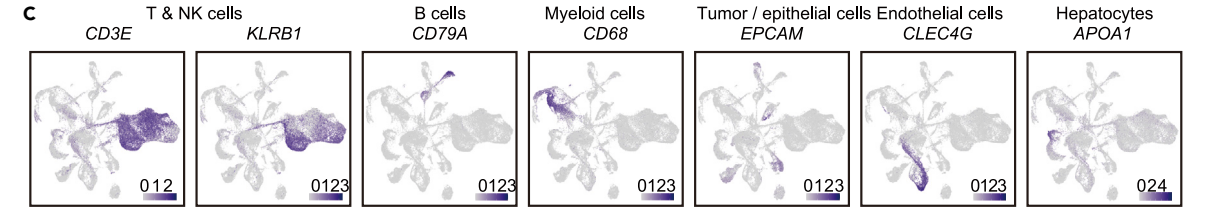
C
T & NK cells
CD3E
KLRB1
B cells
CD79A
Myeloid cells
CD68
Tumor / epithelial cells
EPCAM
Endothelial cells
CLEC4G
Hepatocytes
APOA1

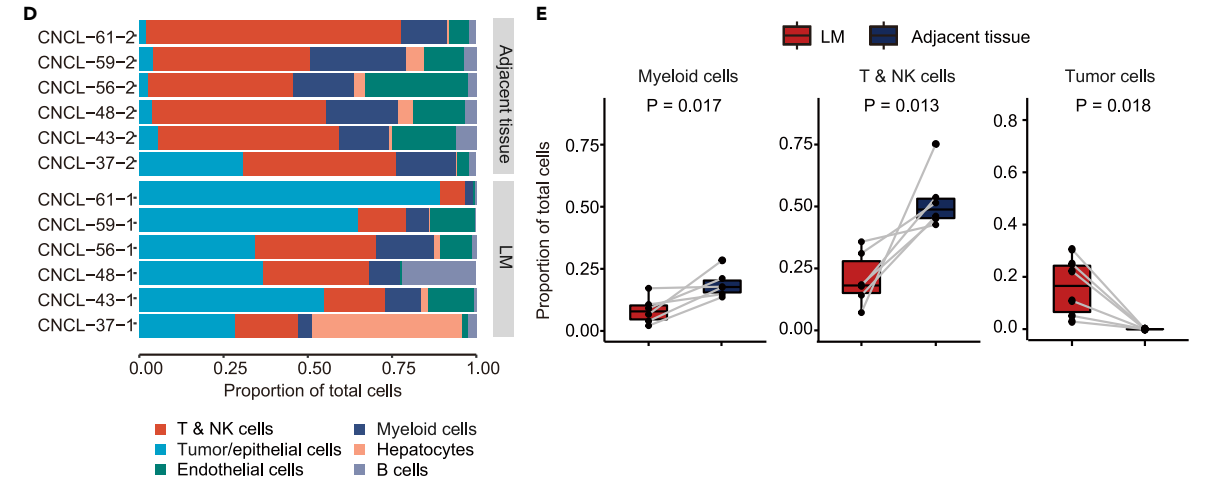
D
CNCL−61−2
CNCL−59−2
CNCL−56−2
CNCL−48−2
CNCL−43−2
CNCL−37−2
CNCL−61−1
CNCL−59−1
CNCL−56−1
CNCL−48−1
CNCL−43−1
CNCL−37−1
Adjacent tissue
LM
Proportion of total cells
T & NK cells
Tumor/epithelial cells
Endothelial cells
Myeloid cells
Hepatocytes
B cells
E
LM
Adjacent tissue
Myeloid cells
P = 0.017
T & NK cells
P = 0.013
Tumor cells
P = 0.018
Proportion of total cells

Figure 1. BRCA LM vs. adjacent tissues

(A) Illustration outlining the processing of single-cell transcriptional analysis.

(B) UMAP plot of total cells from BRCA LMs and adjacent tissues, grouped by cell types, sample sites and sample names.

(C) UMAP plot of marker genes of cell types.

(D) Proportion of cell types among total cells.

(E) Boxplots show proportion of myeloid cell, T & NK cells and tumor cells among total cells. Paired t-test was performed, $p < 0.05$ was considered to be significant.

divided into 3 molecular types: i) luminal group (n = 3), including ER^+ or PR^+; ii) TNBC group (n = 2), including ER^-, PR^- and $HER2^-$; and iii) $HER2^+$ group (n = 1) (Figures 1B; Table S1).

Cell population of LM from BC

Clustering analysis of high-quality transcriptomes obtained from tumor and liver tissue samples was conducted using 10× Genomics. According to Seurat-Guided Clustering Tutorial, we employed a standard pre-processing workflow to process our sequencing data. A total of 70,563 single cells, including 31,996 from the adjacent tissue and 38,567 from the metastatic tumors, were subjected to the Uniform Manifold Approximation and Projection (UMAP) for dimensionality reduction leading to the identification of 6 major cell clusters, including T and natural killer (NK) cells, B cells, tumor and epithelial cells, endothelial cells, myeloid cells, and hepatocytes. We also classified the cells according to the patient origin (Figures 1B and S1A). T & NK cells were identified by the markers *CD3E* and *KLRB1* (25,352 cells), B cells by the marker *CD79A* (2,926 cells), myeloid cells by the marker *CD68* (9,448 cells), and hepatocytes by the marker *APOA1* (4,827 cells) (Figure 1C). Endothelial cells were identified by the marker *CLEC4G* (7,713 cells) and tumor and epithelial cells by the marker *EPCAM* (20,297 cells) (Figure 1C). Tumor (5,920 cells) and epithelial cells (14,377 cells) were also found using CopyKat (Copy-number Karyotyping of Tumors) (Figure S1B).

We found that the trend of alteration in the cell number of the same cell type was relatively consistent (Figures 1D and 1E). Compared with the samples of adjacent liver tissues, that of the metastatic sites contained a decreased proportion of myeloid and T & NK cells, whereas that of tumor cells was elevated (Figure 1E). Overall, different components of the TME were less heterogeneous among patients, showing signs of a commonality.

Heterogeneity of T & NK cells in the TME

Next, we pooled T & NK cells based on the cell type identity and performed clustering analysis to generate a UMAP displaying the phenotypic heterogeneity of each cell type. Seven subclusters were identified among T & NK cells, including NK cells (marker: *KLRB1*), $CD8^+$ NK T cells (markers: *CD3D*, *CD8A* and *IL7R*), $CD8^+$ and major histocompatibility complex (MHC) II^+ T cells (markers: *CD3D*, *CD8A* and *HLA-DRB1*), cytotoxic $CD8^+$ T cells (markers: *CD3D*, *CD8A* and *GZMB*), $CD4^+$ T cells (markers: *CD3D* and *CD4*), and unidentified T cells (markers: *CD3D*, *MALAT1* and *ALB*) (Figures 2A and 2B). The number and proportion of each cell type from all samples are shown in Figure 2C.

Gene Set Enrichment Analysis (GSEA) showed that NK cells in adjacent liver tissues were enriched in leukocyte degranulation and NK cell-mediated immunity, in comparison with those in LM (Figure 2D). As exhibited in Figure S2A, several genes associated with receptors and factors involved in NK cell-mediated killing (such as *KLRB1*, *NKG7*, *KLRF1*, *GZMA*, *KLRD1*, *KLRK1*, *KLRC2*, *GZMK* and *NCR1*) were down-regulated among NK cells in LM and transcriptional analysis of which compared to adjacent tissues showed that NK cell-mediated immunity was decreased.

Meanwhile, T cells in LM also had similar GSEA enrichment results and differential gene expression patterns to NK cells (Figures 2E and 2F). Receptors and factors (*KLRB1*, *KLRD1*, *KLRK1*, *NKG7*, *GZMK*, *KLRC2*, *KLRG1* and *GZMM*) involved in cell killing and proteins regulating T cell activation (*TYROBP*, *XCL2*, *CD48* and *TRAV1-2*) were down-regulated (Figure 2F).

In addition, expression of the co-inhibitory receptor *CTLA4* was up-regulated in LM, indicating negative regulation of T cell activation (Figure 2F). More $CD4^+$ T cell infiltration was found in LM (Figure 2G). Markers of exhausted and regulatory T cells (e.g., *CTLA4*, *TIGIT*, *FOXP3*, *TNFRSF1B* and *TNFRSF18*) were up-regulated among $CD4^+$ T cells in LM. Receptors and proteins (*CD40LG*, *TXNIP*, *PTPRC*, *CD3G*, *XCL1* and *CD48*) related to T cell activation were, however, down-regulated (Figure 2H). These exhausted features of $CD4^+$ T cells point to negative regulation of T cell activation in TME.

$CD8^+$ cytotoxic T cell had a tendency of lower proportion in LM (Figure 2I), while *GZMB* expression was up-regulated that is important for inducing T cell cytotoxicity (Figure 2F). GSEA analysis showed that NK cell-mediated cytotoxicity was down-regulated among $CD8^+$ T cells in LM (Figure 2J). In summary, $CD8^+$ T cells show reduced activation and cytotoxicity.

Transcriptional and cellular landscape of B cells

Both PCA-UMAP and clustering analyses of the scRNA-seq data were utilized to reveal the relationship among B cell subclusters in LM (Figure S1C). *CD79A* is a marker gene for B cells, plasma cells are identified by marker genes *JCHAIN* and *IGHG1*, naive B cells by *HLA-DRA*, and germinal center B cells by *HMGN2*. A new cluster that expresses *CD3E* was found (Figure S1D). Ratio of cell types among B cells and cell fraction analysis demonstrate that $CD3E^+$ B cells were enriched in adjacent tissues (Figures S1E and S1F).

GSEA analysis also showed that immunoglobulin complex and positive regulation of B cell activation were increased, while class II MHC, antigen processing and presentation, as well as B cell regulating T cell-mediated cytotoxicity were all down-regulated (Figure S1G).

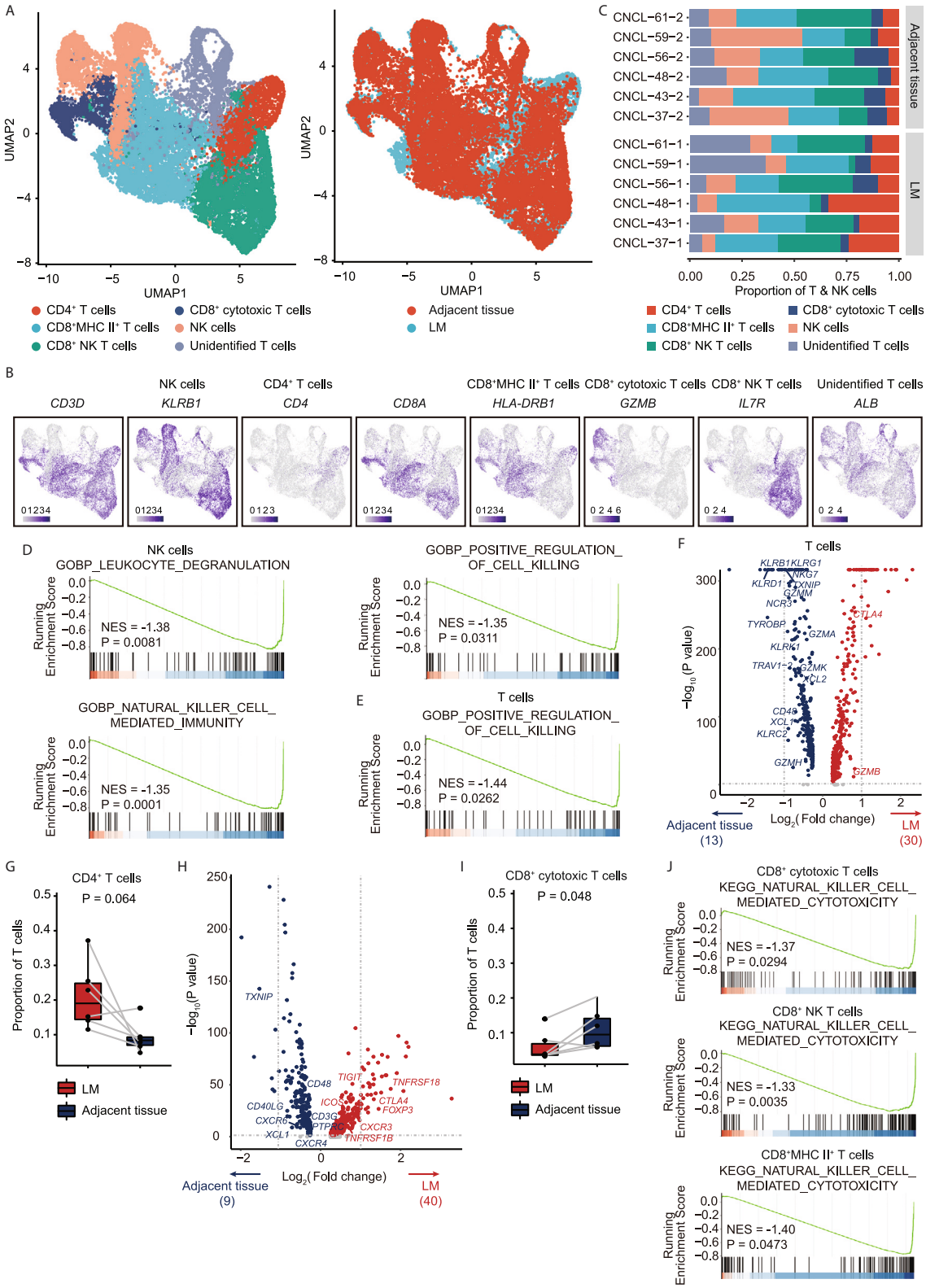

Figure 2. T & NK cells in LM vs. adjacent tissues

(A) UMAP plot of T cells and NK cells, grouped by cell types and sample sites.

(B) UMAP plot of marker genes of subclusters.

Figure 2. *Continued*

(C) Proportion of subclusters among T & NK cells.

(D) GSEA analysis on NK cells in LM vs. adjacent tissues. GSEA plot of GOBP_LEUKOCYTE_DEGRANULATION, GOBP_NATURAL_KILLER_CELL_MEDIATED_IMMUNITY and GOBP_POSITIVE_REGULATION_OF_CELL_KILLING were displayed.

(E) GSEA analysis on T cells in LM vs. adjacent tissues. GSEA plot of GOBP_POSITIVE_REGULATION_OF_CELL_KILLING was displayed.

(F) Volcano plot displays differential genes in T cells between LM (red) and adjacent tissues (blue).

(G) Boxplots show proportion of $CD4^+$ T cells among T cells.

(H) Volcano plot displays differential genes in $CD4^+$ T cells between LM (red) and adjacent tissues (blue).

(I) Boxplots show proportion of $CD8^+$ cytotoxic T cells among T cells.

(J) KEGG_NATURAL_KILLER_CELL_MEDIATED_CYTOTOXICITY enrichment was performed by GSEA in $CD8^+$ cytotoxic T cells, $CD8^+$ NK T cells and $CD8^+$ MHC II^+ T cells between LM and adjacent tissues.

In GSEA analysis results, the p values were adjusted by BM method, adjusted $p < 0.05$ was considered to be significant.

In boxplots, paired t-test was performed, and $p < 0.05$ was considered to be significant.

In differential gene analysis, Wilcoxon Rank-Sum test was used to identifies differentially expressed genes, adjusted $p < 0.05$ was considered to be significant.

Analysis of differential genes between B cells in LM and adjacent tissues displayed that components of class II MHC complex (*HLA-DRA*, *HLA-DRB1*, *HLA-DPA1*, *etc.*) as well as *IGHM* and *IGHD* were down-regulated among B cells in LM, whereas other components such as immunoglobulin (IGHG1, IGKC, *etc.*) were up-regulated (Figure S1H).

Collectively, B cells in the TME of LM shows increased activity of B cell activation, while MHC class II complex, antigen processing and presentation, and B cell regulating T cell-mediated cytotoxicity were decreased.

Accumulation of myeloid cells in adjacent tissues

Myeloid cells include monocytes, macrophages, neutrophils, basophils, eosinophils, erythrocytes, dendritic cells (DCs), megakaryocytes, and platelets, displaying significant cell-to-cell heterogeneity in terms of transcription and secretion patterns.[14] However, the mechanism by which macrophages or DCs became dysregulated in LM remains elusive. We thus performed PCA analysis on myeloid cells using grouped samples from LM and adjacent tissues (Figure 3A). Four myeloid subsets were designated: monocytes with high expression of *FCN1*, neutrophils with high expression of *CXCR2*, macrophages with high expression of *C1QC*, and DCs with high expression of *HLA-DPA1* (Figure 3B). Ratio of myeloid cells showed that cDC1 and $CD3E^+$ macrophages were significantly enriched in adjacent tissue while proliferating DC in LM (Figures S2B and S7).

In the transcription level, GSEA analysis on monocytes showed that signaling pathways related to lymphocyte chemotaxis, chemokine and cytokine activity were up-regulated in LM (Figure S2C). Chemokines (*CCL3L1*, *CCL3*, *CCL4*, *etc.*) and cytokines (GRN and *IL-1B*) was also up-regulated (Figure S2D). GSEA analysis on neutrophils showed that humoral immune response (*C1QA*, *C1QB* and *C1QC*) were down-regulated in LM (Figures S2C and S2E). This result shows that cytokine expression, especially chemokines were up-regulated in monocytes in LM.

We also conducted GSEA analysis on macrophages but no significant macrophage-related pathways were found (Figure S2C). In addition, GSEA analysis on DCs showed that phagocytosis recognition was up-regulated, while T cell activation and MHC II complex were down-regulated (Figure S2C).

In summary, our results show increased cytokine activity and chemotaxis in monocytes. Considering cluster heterogeneity in macrophages and DCs, further sub-clustering was needed to analyze the role of these two types of cells in TME.

Transcriptional characterization of macrophages

Six macrophage clusters were identified in our dataset, including MT^{hi} macrophage (marker gene: *MT-ND4L*), ALB^+ macrophage (marker gene: *ALB*), $FCN3^+$ macrophage (marker gene: *FCN3*), $TREM2^+$ macrophage (marker gene: *TREM2*), $CD163^+$ macrophage (marker gene: *CD163*), and $CD3E^+$ macrophage (marker gene: *CD3E*) (Figures 3C and 3D).

We then performed GO enrichment analysis of marker genes of each subcluster to identify their roles (Figures S3A–S3F). Pathways related to immunity were enriched in $CD163^+$ (Figure S3A), $TREM2^+$ (Figure S3B) and $FCN3^+$ (Figure S3C) macrophages. Therefore, further analysis was performed to investigate the changes of these 3 subclusters between LM and adjacent tissues.

It was reported that $CD163^+$ macrophages are pro-inflammatory.[15] Signaling pathways of this subcluster were enriched in neutrophil activation, neutrophil degranulation and antigen processing and presentation (Figure S3A). However, only pathway of the immunoglobulin complex was enriched among $CD163^+$ macrophages in LM compared to that in adjacent liver tissues (Figure 3E).

Tumor-associated monocytes/macrophages with TREM2 high expression exhibits potent immunosuppressive activity.[16] Pathways of this subcluster were enriched in neutrophil activation, neutrophil degranulation and antigen processing and presentation as well (Figure S3B). GSEA analysis showed that both chemokine and cytokine expression were up-regulated among $TREM2^+$ macrophages in LM (Figure 3E).

$FCN3^+$ macrophages have not been reported previously. In their GO enrichment analysis, receptor-mediated endocytosis was enriched, indicating that it may participate in endocytosis-mediated antigen clearing and processing (Figure S3C). GSEA analysis showed that complement activation, scavenger receptor expression and positive regulation of cell killing were down-regulated among $FCN3^+$ macrophages in LM (Figure 3E).

It appears that the two subclusters ($TREM2^+$ and $FCN3^+$) of macrophages may form an immunosuppressive TME possibly related to tumor cell seeding in the liver.

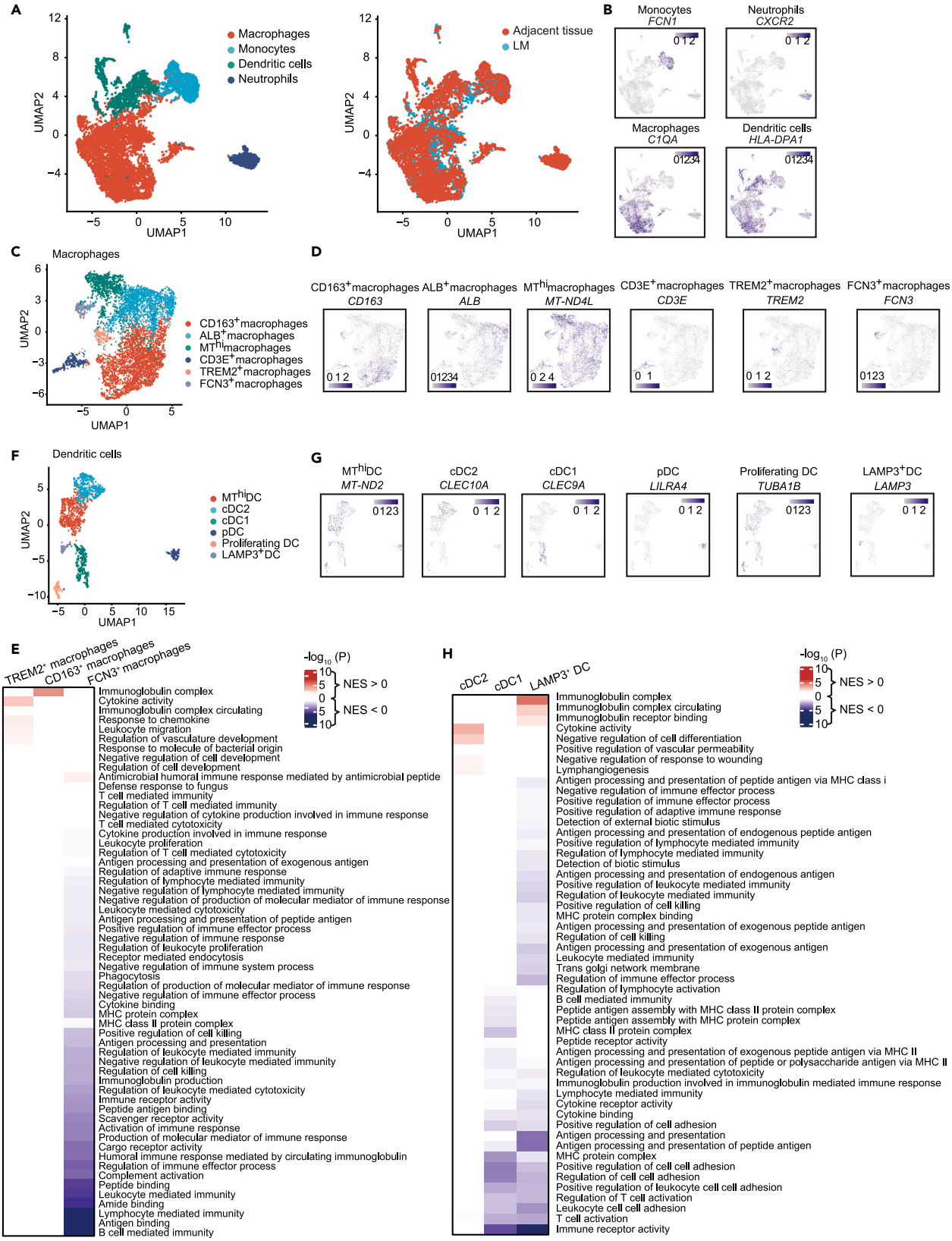
A
Macrophages
Monocytes
Dendritic cells
Neutrophils
Adjacent tissue
LM
UMAP1
UMAP2
B
Monocytes
FCN1
Neutrophils
CXCR2
Macrophages
C1QA
Dendritic cells
HLA-DPA1
C
Macrophages
CD163+macrophages
ALB+macrophages
MThimacrophages
CD3E+macrophages
TREM2+macrophages
FCN3+macrophages
D
CD163+macrophages
CD163
ALB+macrophages
ALB
MThimacrophages
MT-ND4L
CD3E+macrophages
CD3E
TREM2+macrophages
TREM2
FCN3+macrophages
FCN3
F
Dendritic cells
MThiDC
cDC2
cDC1
pDC
Proliferating DC
LAMP3+DC
G
MThiDC
MT-ND2
cDC2
CLEC10A
cDC1
CLEC9A
pDC
LILRA4
Proliferating DC
TUBA1B
LAMP3+DC
LAMP3
E
TREM2+ macrophages
CD163+ macrophages
FCN3+ macrophages
-log10 (P)
NES > 0
NES < 0
Immunoglobulin complex
Cytokine activity
Immunoglobulin complex circulating
Response to chemokine
Leukocyte migration
Regulation of vasculature development
Response to molecule of bacterial origin
Negative regulation of cell development
Regulation of cell development
Antimicrobial humoral immune response mediated by antimicrobial peptide
Defense response to fungus
T cell mediated immunity
Regulation of T cell mediated immunity
Negative regulation of cytokine production involved in immune response
T cell mediated cytotoxicity
Cytokine production involved in immune response
Leukocyte proliferation
Regulation of T cell mediated cytotoxicity
Antigen processing and presentation of exogenous antigen
Regulation of adaptive immune response
Regulation of lymphocyte mediated immunity
Negative regulation of lymphocyte mediated immunity
Negative regulation of production of molecular mediator of immune response
Leukocyte mediated cytotoxicity
Antigen processing and presentation of peptide antigen
Positive regulation of immune effector process
Negative regulation of immune response
Regulation of leukocyte proliferation
Receptor mediated endocytosis
Negative regulation of immune system process
Phagocytosis
Regulation of production of molecular mediator of immune response
Negative regulation of immune effector process
Cytokine binding
MHC protein complex
MHC class II protein complex
Positive regulation of cell killing
Antigen processing and presentation
Regulation of leukocyte mediated immunity
Negative regulation of leukocyte mediated immunity
Regulation of cell killing
Immunoglobulin production
Regulation of leukocyte mediated cytotoxicity
Immune receptor activity
Peptide antigen binding
Scavenger receptor activity
Activation of immune response
Production of molecular mediator of immune response
Cargo receptor activity
Humoral immune response mediated by circulating immunoglobulin
Regulation of immune effector process
Complement activation
Peptide binding
Leukocyte mediated immunity
Amide binding
Lymphocyte mediated immunity
Antigen binding
B cell mediated immunity
H
cDC2
cDC1
LAMP3+ DC
-log10 (P)
NES > 0
NES < 0
Immunoglobulin complex
Immunoglobulin complex circulating
Immunoglobulin receptor binding
Cytokine activity
Negative regulation of cell differentiation
Positive regulation of vascular permeability
Negative regulation of response to wounding
Lymphangiogenesis
Antigen processing and presentation of peptide antigen via MHC class i
Negative regulation of immune effector process
Positive regulation of immune effector process
Positive regulation of adaptive immune response
Detection of external biotic stimulus
Antigen processing and presentation of endogenous peptide antigen
Positive regulation of lymphocyte mediated immunity
Regulation of lymphocyte mediated immunity
Detection of biotic stimulus
Antigen processing and presentation of endogenous antigen
Positive regulation of leukocyte mediated immunity
Regulation of leukocyte mediated immunity
Positive regulation of cell killing
MHC protein complex binding
Antigen processing and presentation of exogenous peptide antigen
Regulation of cell killing
Antigen processing and presentation of exogenous antigen
Leukocyte mediated immunity
Trans golgi network membrane
Regulation of immune effector process
Regulation of lymphocyte activation
B cell mediated immunity
Peptide antigen assembly with MHC class II protein complex
Peptide antigen assembly with MHC protein complex
MHC class II protein complex
Peptide receptor activity
Antigen processing and presentation of exogenous peptide antigen via MHC II
Antigen processing and presentation of peptide or polysaccharide antigen via MHC II
Regulation of leukocyte mediated cytotoxicity
Immunoglobulin production involved in immunoglobulin mediated immune response
Lymphocyte mediated immunity
Cytokine receptor activity
Cytokine binding
Positive regulation of cell adhesion
Antigen processing and presentation
Antigen processing and presentation of peptide antigen
MHC protein complex
Positive regulation of cell cell adhesion
Regulation of cell cell adhesion
Positive regulation of leukocyte cell cell adhesion
Regulation of T cell activation
Leukocyte cell cell adhesion
T cell activation
Immune receptor activity

Figure 3. Macrophages and dendritic cells in LM vs. adjacent tissues

(A) UMAP plot of myeloid cells, grouped by subclusters and sample sites.

(B) UMAP plot of marker genes of subclusters.

(C) UMAP plot of macrophages, grouped by subclusters.

(D) UMAP plot of marker genes of subclusters.

(E) GSEA analysis on CD163$^+$ macrophages, TREM2$^+$ macrophages and FCN3$^+$ macrophages in LM (red) vs. adjacent tissues (blue).

(F) UMAP plot of dendritic cells, grouped by subclusters.

(G) UMAP plot of marker genes of subclusters.

(H) GSEA analysis on cDC2, LAMP3$^+$ DC and cDC1 in LM (red) vs. adjacent tissues (blue).

In GSEA analysis, the p values were adjusted by BM method, adjusted $p < 0.05$ was considered to be significant and colored.

Transcriptional characterization of dendritic cells

The primary function of DCs in cancer immunity is to acquire and present tumor antigen to T cells. We carried out clustering analysis that identified five DC clusters: MT^{hi} DC by marker gene *MT-ND2*, cDC2 by *CLEC10A*, type 1 conventional dendritic cell (cDC1) by *CLEC9A*, plasmacytoid dendritic cell (pDC) by *LILRA4*, proliferating DC by *TUBA1B*, and LAMP3$^+$ DC by *LAMP3* (Figures 3F and 3G).

These marker genes were then used in GO enrichment analysis to define their roles (Figures S3G–S3L). Pathways related to immunity were enriched in cDC2 (Figure S3G) and LAMP3$^+$ DC (Figure S3H). cDC1 was reported to be related to immunity.[17] Therefore, even though it was not shown in the GO analysis (Figure S3I), further analysis was still carried out on cDC1 as well as on cDC2 and activating DC to investigate the differences among these 3 subclusters.

cDC2 plays an important role in antigen presentation via interaction with CD4$^+$ T cells.[18] In its GO analysis, T cell activation, leukocyte adhesion and proliferation were enriched (Figure S3G), while GSEA showed that cytokine expression and negative regulation of vasculature were up-regulated in LM (Figure 3H).

LAMP3$^+$ mature DCs usually found in tumor were reported to regulate multiple subtypes of lymphocytes, including interaction with CD4$^+$ and CD8$^+$ T cells.[19] In the GO analysis of LAMP3$^+$ DCs, NFKB, IFNγ, TNF and IL-12 signaling were enriched (Figure S3H), indicative of DC maturation.[20] GSEA analysis showed that regulation of T cell activation as well as antigen processing and presentation were down-regulated in LM (Figure 3H).

cDC1 is mainly responsible for antigen presentation to activating immune responses.[21] In the GO analysis, however, pathways in antigen presentation were not found among the top 10 enrichments in cDC1 marker genes (Figure S3I). GSEA analysis showed that cytokine production, regulation of T cell activation and MHC II complex were down-regulated in LM (Figure 3H).

Collectively, in LM, cDC2 shows decreased cytokines expression, LAMP3$^+$ DCs demonstrate reduced regulation of T cell activation as well as antigen processing and presentation, and cDC1 has down-regulated cytokine expression, T cell activation and antigen processing and presentation, suggesting these DC subtypes may modulate T cell activity to promote tumor cell seeding in the Liver.

Association of macrophages with CD4$^+$ T cell infiltration

Higher infiltration of CD4$^+$ T cells were found in LM, especially those with exhausted and regulatory markers (Figures 2G, 2H, and S3). This was accompanied by elevated expression of *CXCR3* among CD4$^+$ T cells in LM as well as *CXCR6* and *CXCR4* in the adjacent tissue (Figure 2H).

To explore the profile of CD4$^+$ T cell in LM and adjacent tissues, we performed a trajectory analysis based on the pseudo-time branching algorithm. According to the split pseudo-time trajectory, CD4$^+$ T cells displayed different characteristics between LM and the adjacent tissue (Figure S4A). Exhausted and regulatory markers, *TIGIT*, *CTLA4*, *PDCD1* and *FOXP3*, were mainly located in the same branch (Figure S4B), where *CXCR3* was also located (Figure S4C). Meanwhile, elevated expression of *CXCR4* was largely found in CD4$^+$ T cells without exhausted and regulatory markers (Figure S4C).

CXCL12 and CXCL9/10/11 are key ligands of CXCR4 and CXCR3, respectively.[22,23] These four chemokines are expressed in macrophages (Figure S4D). Macrophages in the adjacent tissue expressed a significantly higher level of *CXCR12* (Figure S4E). In addition, a possible CXCL12-CXCR4 interaction was shown between macrophages and CD4$^+$ T cells in the adjacent tissue (Figure S4F). CXCL9/10/11 expressions were up-regulated among macrophages in LM (Figure S4E), and the CXCL9/10/11-CXCR3 interaction was only observed in LM (Figure S4F).

Our data support a predominantly linear trajectory associated with progressive CD4$^+$ T cell exhaustion and interactions between CD4$^+$ T cells and macrophages. In summary, macrophages may enhance infiltration of CD4$^+$ T cells without exhausted markers through the CXCL12-CXCR4 axis in the adjacent tissue, and infiltration of exhausted CD4$^+$ T cells through the CXCL9/10/11-CXCR3 axis only exist in LM.

T cell functions regulated by FCN3$^+$ macrophage, cDC1 and LAMP3$^+$ DC

We previously noticed dysfunction of T cells in LM (Figure 2J). Antigen processing and presentation by APC is an essential step to initiate T cell immunity. DCs, macrophages and B cells are the principal antigen-presenting cells for T cells. In GSEA, we found that FCN3$^+$ macrophages (Figure 4A), cDC1 (Figure 4B) and LAMP3$^+$ DCs (Figure 4C) in LM negatively regulated T cell-mediated cytotoxicity and T cell activation, and their ability of antigen processing and presentation was down-regulated. To quantify antigen presentation function, MHC components that were expressed in over 30% cells (boxed in Figure S2F) were included to calculate MHC signature scores. Both MHC signature scores and

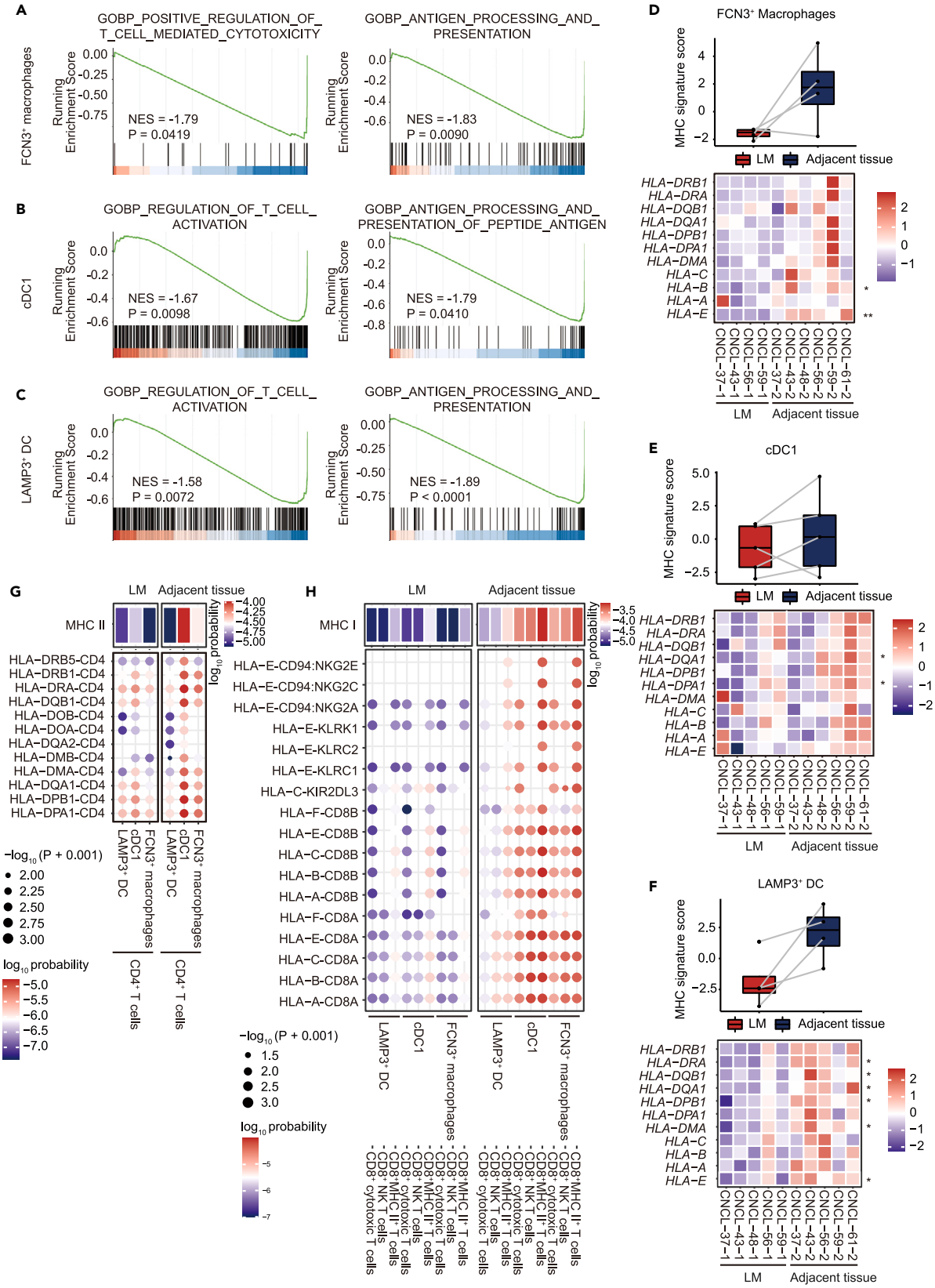
A
GOBP_POSITIVE_REGULATION_OF_T_CELL_MEDIATED_CYTOTOXICITY
GOBP_ANTIGEN_PROCESSING_AND_PRESENTATION
FCN3+ macrophages
Running Enrichment Score
NES = -1.79
P = 0.0419
NES = -1.83
P = 0.0090
B
GOBP_REGULATION_OF_T_CELL_ACTIVATION
GOBP_ANTIGEN_PROCESSING_AND_PRESENTATION_OF_PEPTIDE_ANTIGEN
cDC1
NES = -1.67
P = 0.0098
NES = -1.79
P = 0.0410
C
GOBP_REGULATION_OF_T_CELL_ACTIVATION
GOBP_ANTIGEN_PROCESSING_AND_PRESENTATION
LAMP3+ DC
NES = -1.58
P = 0.0072
NES = -1.89
P < 0.0001
D
FCN3+ Macrophages
MHC signature score
LM
Adjacent tissue
HLA-DRB1
HLA-DRA
HLA-DQB1
HLA-DQA1
HLA-DPB1
HLA-DPA1
HLA-DMA
HLA-C
HLA-B
HLA-A
HLA-E
CNCL-37-1
CNCL-43-1
CNCL-56-1
CNCL-59-1
CNCL-37-2
CNCL-43-2
CNCL-48-2
CNCL-56-2
CNCL-59-2
CNCL-61-2
E
cDC1
F
LAMP3+ DC
G
MHC II
HLA-DRB5-CD4
HLA-DRB1-CD4
HLA-DRA-CD4
HLA-DQB1-CD4
HLA-DOB-CD4
HLA-DOA-CD4
HLA-DQA2-CD4
HLA-DMB-CD4
HLA-DMA-CD4
HLA-DQA1-CD4
HLA-DPB1-CD4
HLA-DPA1-CD4
LAMP3+ DC
cDC1
FCN3+ macrophages
CD4+ T cells
log10 probability
−log10 (P + 0.001)
H
MHC I
HLA-E-CD94:NKG2E
HLA-E-CD94:NKG2C
HLA-E-CD94:NKG2A
HLA-E-KLRK1
HLA-E-KLRC2
HLA-E-KLRC1
HLA-C-KIR2DL3
HLA-F-CD8B
HLA-E-CD8B
HLA-C-CD8B
HLA-B-CD8B
HLA-A-CD8B
HLA-F-CD8A
HLA-E-CD8A
HLA-C-CD8A
HLA-B-CD8A
HLA-A-CD8A
CD8+ cytotoxic T cells
CD8+ NK T cells
CD8+ MHC II+ T cells

Figure 4. FCN3$^+$ macrophage, cDC1 and LAMP3$^+$ DC regulated T cell functions, probably by antigen processing and presentation

(A–C) Enrichment of pathways involved in antigen presentation and regulation of T cell functions were estimated by GSEA in FCN3$^+$ macrophages (A), cDC1 (B) and LAMP3$^+$ DC (C) between LM and adjacent tissues.

(D–F) Boxplots show MHC GSVA signature score and heatmaps show expression of MHC components in FCN3$^+$ macrophages (D), cDC1 (E) and LAMP3$^+$ DC (F) among samples.

(G) Cell-cell interaction between FCN3$^+$ macrophages, cDC1 and LAMP3$^+$ DC and CD4$^+$ T cells in MHC II pathway.

(H) Cell-cell interaction between FCN3$^+$ macrophages, cDC1 and LAMP3$^+$ DC and CD8$^+$ T cells in MHC I pathway.

In gene expression analysis, paired t-test was performed. $p < 0.05$*, $p < 0.01$**, $p < 0.001$***, $p < 0.0001$****.

In cell-cell interaction analysis, the heatmap above shows probability of interaction in the whole pathway, while the bubble plot shows those in each receptor-ligand pair.

expression values demonstrated that expression of components of MHC tended lower among these cells in LM (Figures 4D–4F). Therefore, we hypothesize that these cells regulate T cell functions by antigen processing and presentation.

To verify this hypothesis, we studied the ligand-receptor (L-R) interaction between these three clusters and T cells to identify potential links that may affect cytotoxicity of the latter in LM and adjacent tissues. In MHC II pathway, the probability of the whole pathway and each L-R interaction were larger between FCN3$^+$ macrophages, cDC1 and CD4$^+$ T cells in the adjacent tissue (Figure 4G). However, in MHC II pathway between LAMP3$^+$ DC and CD4$^+$ T cells, the number of interaction was larger in the adjacent tissue, while the probability of the whole pathway and most L-R interactions were smaller in the adjacent tissue (Figure 4G). In MHC I pathway, the probability of the whole pathway, each L-R interaction and the number of interactions were larger between FCN3$^+$ macrophage, cDC1, LAMP3$^+$ DC and CD8$^+$ T cells in the adjacent tissue (Figure 4H).

To estimate the importance of MHC signal, we computed signaling changes of FCN3$^+$ macrophage, cDC1, LAMP3$^+$ DC and T cells between adjacent tissue and LM. In T cells, MHC-I signal had the largest differential incoming interaction strength and higher strength was shown in the adjacent tissue (Figure S8A). In FCN3$^+$ macrophage, cDC1 and LAMP3$^+$ DC, MHC-I and MHC-II signals had much larger differential outgoing interaction strength and higher strength was shown in the adjacent tissue (Figure S8A). These results indicates that between the adjacent tissue and LM, the changes of T cells may be mainly made through MHC-I pathway, and MHC-I and MHC-II signals were the most important changes of FCN3$^+$ macrophage, cDC1 and LAMP3$^+$ DC in cell interaction. To further explore the importance of MHC signal in cell interaction between T cells and FCN3$^+$ macrophage, cDC1 and LAMP3$^+$ DC, all pathway interaction strength were mapped in Figure S8B. We found that MHC-I and MHC-II pathway interactions had high strengths in both adjacent tissues and LM, showing the importance (Figure S8B). Corresponded to the former results, higher MHC-I and MHC-II pathway interaction strengths were shown in the adjacent tissue (Figure S8B). In addition, cell adhesion pathways (GALECTIN and ICAM) and co-stimulatory signaling pathway (CD40, CD86 and CD80), which benefit antigen presentation, were also shown stronger interaction in the adjacent tissue (Figure S8B).

Altogether, our data demonstrate that FCN3$^+$ macrophages, cDC1 and LAMP3$^+$ DC could regulate CD4$^+$ and CD8$^+$ T cells, probably via MHC I and II presentation.

Sc-RNA sequencing of LM originating from NPC, THCA and CESC

To verify the general relevance of mechanisms we found in BC, we performed sc-RNA sequencing of LM and adjacent tissues from patients with NPC (2 cases, 21,937 cells) (Figures 5A and S5A), THCA (2 cases, 43,402 cells) (Figures 5B and S5C) and CESC (1 cases, 13,780 cells) (Figures 5C and S5E). We extracted T cells (marker: *CD3E*) and identified as CD4$^+$ T cells (marker: *CD4*) and CD8$^+$ T cells (marker: *CD8B*) (Figures 5A–5C, S5B, S5D, and S5F). We also extracted myeloid cells (marker: *CD68*) and identified as cDC1 (marker: *CLEC9A*) and macrophages (marker: *C1QA*) (Figures 5A–5C, S5B, S5D, and S5F).

In NPC, CD4$^+$ T cell profile with similar to that of BC was displayed. Exhausted CD4$^+$ T cells were mainly found in LM, and *CXCR3* was located in exhausted CD4$^+$ T cells, while *CXCR4* was mainly located in those without exhausted markers (Figure S5G). Different from NPC and BC, in THCA and CESC, few CD4$^+$ T cells with exhausted markers and *CXCR3* were found, and almost all CD4$^+$ T cells expressed *CXCR4* (Figures S5H and S5I).

CXCL12-CXCR4 interaction between macrophages and CD4$^+$ T cells was stronger in adjacent tissues in three cancers (Figure S5J). Higher levels of *CXCL12* shown in macrophages in the adjacent tissue also verified stronger CXCL12-CXCR4 interaction (Figure S5K). However, stronger CXCL9/10/11-CXCR3 interaction was only discovered in LM of NPC, instead of THCA and CESC (Figure S5J), probably because of little infiltration of exhausted CD4$^+$ T cells in the latter two cancers (Figures S5H and S5I). In addition, *CXCL9/10/11* were highly expressed in macrophages in NPC-LM (Figure S5K).

In NPC, THCA and CESC, most pairs of samples showed the same tendency that adjacent tissues had higher cDC1 ratios than LM, except for CNCL-55, a pair of NPC (Figure 5D). In these three cancers, stronger interactions of MHC I and MHC II pathway between cDC1 and T cells were discovered in adjacent tissues (Figures 5E and 5F). In NPC and CESC, MHC signature scores and most components were up-regulated in cDC1 in adjacent tissues, while in THCA, signature scores of a pair of samples present an opposite trend but some components of MHC were still up-regulated (Figure 5G). FCN3$^+$ macrophages and LAMP3$^+$ macrophages were not found in these three cancers, probably due to small sample size.

In conclusion, mechanisms involved in macrophages altering CD4$^+$ T cell profile and cDC1 antigen presentation were verified not only in BC, but also in NPC, THCA and CESC, indicating the general relevance of these mechanisms.

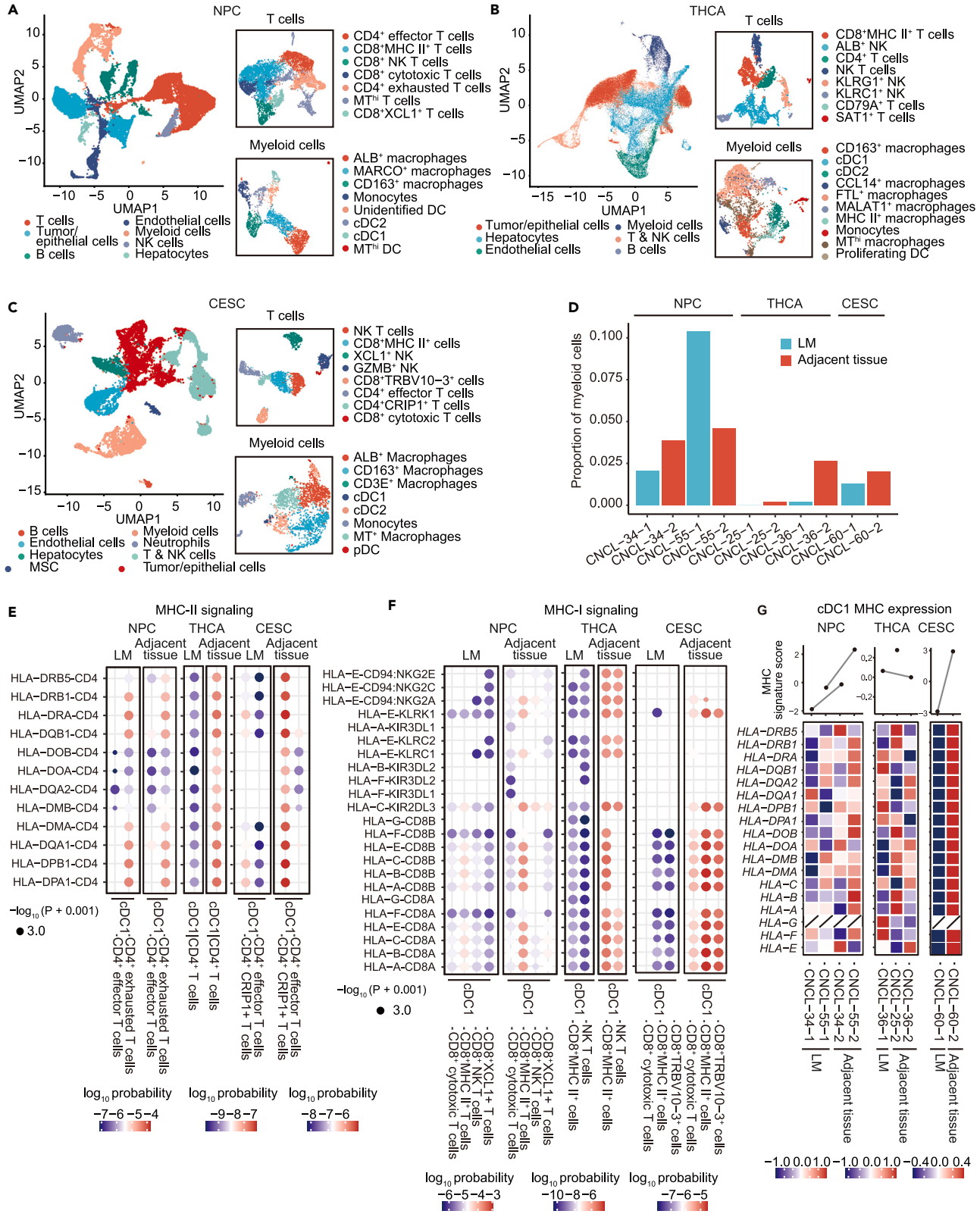
A
NPC
T cells
Myeloid cells
UMAP1
UMAP2
T cells
Tumor/epithelial cells
B cells
Endothelial cells
Myeloid cells
NK cells
Hepatocytes
CD4+ effector T cells
CD8+MHC II+ T cells
CD8+ NK T cells
CD8+ cytotoxic T cells
CD4+ exhausted T cells
MThi T cells
CD8+XCL1+ T cells
ALB+ macrophages
MARCO+ macrophages
CD163+ macrophages
Monocytes
Unidentified DC
cDC2
cDC1
MThi DC
B
THCA
T cells
Myeloid cells
Tumor/epithelial cells
Hepatocytes
Endothelial cells
Myeloid cells
T & NK cells
B cells
CD8+MHC II+ T cells
ALB+ NK
CD4+ T cells
NK T cells
KLRG1+ NK
KLRC1+ NK
CD79A+ T cells
SAT1+ T cells
CD163+ macrophages
cDC1
cDC2
CCL14+ macrophages
FTL+ macrophages
MALAT1+ macrophages
MHC II+ macrophages
Monocytes
MThi macrophages
Proliferating DC
C
CESC
T cells
Myeloid cells
B cells
Endothelial cells
Hepatocytes
MSC
Myeloid cells
Neutrophils
T & NK cells
Tumor/epithelial cells
NK T cells
CD8+MHC II+ cells
XCL1+ NK
GZMB+ NK
CD8+TRBV10−3+ cells
CD4+ effector T cells
CD4+CRIP1+ T cells
CD8+ cytotoxic T cells
ALB+ Macrophages
CD163+ Macrophages
CD3E+ Macrophages
cDC1
cDC2
Monocytes
MT+ Macrophages
pDC
D
NPC
THCA
CESC
LM
Adjacent tissue
Proportion of myeloid cells
CNCL−34−1
CNCL−34−2
CNCL−55−1
CNCL−55−2
CNCL−25−1
CNCL−25−2
CNCL−36−1
CNCL−36−2
CNCL−60−1
CNCL−60−2
E
MHC-II signaling
NPC
THCA
CESC
LM
Adjacent tissue
HLA−DRB5−CD4
HLA−DRB1−CD4
HLA−DRA−CD4
HLA−DQB1−CD4
HLA−DOB−CD4
HLA−DOA−CD4
HLA−DQA2−CD4
HLA−DMB−CD4
HLA−DMA−CD4
HLA−DQA1−CD4
HLA−DPB1−CD4
HLA−DPA1−CD4
−log10 (P + 0.001)
3.0
cDC1|CD4+ exhausted T cells
cDC1|CD4+ effector T cells
cDC1|CD4+ T cells
cDC1|CD4+ effector T cells CRIP1+ T cells
cDC1|CD4+ effector T cells CRIP1+ T cells
log10 probability
−7−6 −5−4
−9−8−7
−8−7−6
F
MHC-I signaling
NPC
THCA
CESC
LM
Adjacent tissue
HLA−E−CD94:NKG2E
HLA−E−CD94:NKG2C
HLA−E−CD94:NKG2A
HLA−E−KLRK1
HLA−A−KIR3DL1
HLA−E−KLRC2
HLA−E−KLRC1
HLA−B−KIR3DL2
HLA−F−KIR3DL2
HLA−F−KIR3DL1
HLA−C−KIR2DL3
HLA−G−CD8B
HLA−F−CD8B
HLA−E−CD8B
HLA−C−CD8B
HLA−B−CD8B
HLA−A−CD8B
HLA−G−CD8A
HLA−F−CD8A
HLA−E−CD8A
HLA−C−CD8A
HLA−B−CD8A
HLA−A−CD8A
−log10 (P + 0.001)
3.0
cDC1 - CD8+ cytotoxic T cells
cDC1 - CD8+NK T cells
cDC1 - CD8+MHC II+ T cells
cDC1 - CD8+XCL1+ T cells
cDC1 - NK T cells
cDC1 - CD8+MHC II+ cells
cDC1 - CD8+ cytotoxic T cells
cDC1 - CD8+TRBV10−3+ cells
log10 probability
−6−5−4−3
−10−8−6
−7−6−5
G
cDC1 MHC expression
NPC
THCA
CESC
MHC signature score
HLA−DRB5
HLA−DRB1
HLA−DRA
HLA−DQB1
HLA−DQA2
HLA−DQA1
HLA−DPB1
HLA−DPA1
HLA−DOB
HLA−DOA
HLA−DMB
HLA−DMA
HLA−C
HLA−B
HLA−A
HLA−G
HLA−F
HLA−E
CNCL−34−1
CNCL−55−1
CNCL−34−2
CNCL−55−2
CNCL−36−1
CNCL−25−2
CNCL−36−2
CNCL−60−1
CNCL−60−2
LM
Adjacent tissue
−1.0 0.0 1.0
−1.0 0.0 1.0
−0.4 0.0 0.4

Figure 5. sc-RNA sequencing of LM and adjacent tissue originating from NPC, THCA and CESC

(A) UMAP plot of total cells, T cells and myeloid cells from NPC-LMs and adjacent tissues, grouped by cell types.

(B) UMAP plot of total cells, T cells and myeloid cells from THCA-LMs and adjacent tissues, grouped by cell types.

(C) UMAP plot of total cells, T cells and myeloid cells from CESC-LMs and adjacent tissues, grouped by cell types.

(D) Proportion of cDC1 among myeloid cells in NPC, THCA and CESC.

(E) Cell-cell interaction between cDC1 and $CD4^+$ T cells in MHC II pathway and between cDC1 and $CD8^+$ T cells in MHC II pathway in NPC, THCA and CESC.

(F) Cell-cell interaction between cDC1 and $CD4^+$ T cells in MHC I pathway and between cDC1 and $CD8^+$ T cells in MHC I pathway in NPC, THCA and CESC.

(G) Boxplots showed MHC signature scores and heatmaps show expression of MHC components in cDC1 among samples of NPC, THCA and CESC.

Clinical verification of alteration and function of $FCN3^+$ macrophage, cDC1 and $LAMP3^+$ DC in LM

To check the MHC alteration of $FCN3^+$ macrophage, cDC1 and $LAMP3^+$ DC in protein levels, we performed immunofluorescence on a tissue array that contains sections sampled from patients with BC. Patient and section information was listed in Table S2. LM had lower proportion of $FCN3^+C1QC^+HLA\text{-}E^+$ cells, $XCR1^+HLA\text{-}E^+$ cells, $XCR1^+HLA\text{-}DQA1^+$ cells, $XCR1^+HLA\text{-}DPA1^+$ cells and $LAMP3^+HLA\text{-}E^+$ cells compared with primary tumor of invasive ductal breast carcinoma (above phase 3C, staged by AJCC 6^{th} Edition) and normal mammary ducts or lobules (Figures 6A, 6B, and S6A–S6C).

Next, we compared survival of patients with high and low MHC signature scores. To specify the role of MHC genes in our target cells, we need to divide patients into two groups as $FCN3^+$ macrophages, cDC1 and $LAMP3^+$ DC enriched and non-enriched patients and perform survival analysis separately. We explored the expression pattern of marker genes *FCN3*, *C1QC*, *XCR1* and *LAMP3* in all sub-types of cells. We found that *XCR1* and *LAMP3* were only expressed in cDC1 and $LAMP3^+$ DC accounting for 50%–75% of these cell types (Figure S8C), leading to low chance to be interfered by other sub-types, making it possible to indicate the levels of cDC1 and $LAMP3^+$ DC in samples. Except for $FCN3^+$ macrophages, *FCN3* was also expressed in endothelial cells but without CIQC (Figure S8C). Therefore, to lower the interference of endothelial cells, we used two genes (*FCN3* and *C1QC*) to calculate GSVA scores as indication of levels of $FCN3^+$ macrophages in samples. Median value was used to split the patient.

In TCGA BRCA cohort, only in patients enriched with cDC1 and $LAMP3^+$ DC, higher MHC signature score was related to better overall survival (OS) (Figure 6C). In liver cancer, in patients enriched with $LAMP3^+$ DC, higher MHC signature score was related to better overall survival (OS), especially in the early stage (Figure 6D).

In summary, MHC levels in $FCN3^+$ macrophages, cDC1 and $LAMP3^+$ DC were downregulated in LM and some of MHC genes in these cells were linked with survival in BC and liver cancer.

DISCUSSION

In this work, we used scRNA-seq to identify key immune cells and studied their functional roles in the TME of BC-LM at a single-cell resolution. We presented the cellular landscape and transcriptional features of T cells, B cells and myeloid cells in both LM and adjacent tissues. More importantly, for the first time, we provided a dynamic and comprehensive L-R interaction map in myeloid cells to illustrate the presence of reprogrammed profile of $CD4^+$ T cells and cytotoxicity of $CD8^+$ T cells in the TME of BC-LM. This analysis identified multiple significant cell-cell interactions forming a two-side effect in LM, whereby macrophages express ligands for recruiting exhausted $CD4^+$ T cells and meanwhile produce less chemokines for non-exhausted $CD4^+$ T cell infiltration. This is accompanied by reduced antigen presentation to multiple $CD8^+$ T cells by $FCN3^+$ macrophages, cDC1 and $LAMP3^+$ DCs.

Macrophages are involved in regulatory $CD4^+$ T cell infiltration and linked with poor responses and prognosis of cancer.[24,25] In this study, we found that they altered migration of $CD4^+$ T cell with different functions via the CXCL12-CXCR4 and CXCL9/10/11-CXCR3 interactions. In our previous knowledge, *CXCR3* and *CXCR4* are highly expressed on Treg, and targeting these chemokine receptors can revert the immunosuppression of Treg.[26,27] The role of *CXCR3* in Treg is consistent with our discovery. However, we found that compared to exhausted $CD4^+$ T cells, those without exhausted and regulatory profile expressed higher level of *CXCR4*, leading to a new view of *CXCR4* in immune activity of $CD4^+$ T cells.

It seems that the method of enhancing antigen presentation in LM is still unclear and the clinical relevance of antigen presentation in metastatic cancer has not been reported previously. Based on the phenotypic alteration observed, we deduce that compared with adjacent tissues, tumor cells show reduced tumor antigen releases. Our findings suggest that reduced antigen presentation is common among T, B and myeloid cells in LM vs. adjacent tissues, especially among $FCN3^+$ macrophages, cDC1 and $LAMP3^+$ DCs. Thus, this study establishes an association of antigen presentation with malignancy in BC-LM.

$FCN3^+$ macrophages have not been reported. We demonstrated that $FCN3^+$ macrophages may inhibit T cell-mediated cytotoxicity. In terms of signaling pathways, our data show that MHC I and II involvement may play a key role. We believe that decreases in $CD8^+$ T cytotoxicity facilitate tumor cell seeding in the liver and targeting the related pathways may help treat BC-LM with poor immune infiltration by enhancing antigen processing and presentation to reactivate $CD8^+$ T cells.

cDC1 and $LAMP3^+$ DCs are capable of performing cross-presentation for cytotoxic $CD8^+$ T cell priming and activation. However, their role in LM is still elusive. Nonetheless, reduction of cytotoxic $CD8^+$ T cells in LM would certainly pave the way for BC seeding in the liver. Thus, enhancing antigen presentation might help treat BC-LM with poor immune infiltration.

Together, we report here a reprogrammed profile of T cells in BC-LM altered by myeloid cells, i.e., macrophages affect $CD4^+$ T cell infiltration in the TME and $FCN3^+$ macrophages, cDC1 and $LAMP3^+$ DC down-regulate antigen presentation to reduce activation of $CD8^+$ T cells

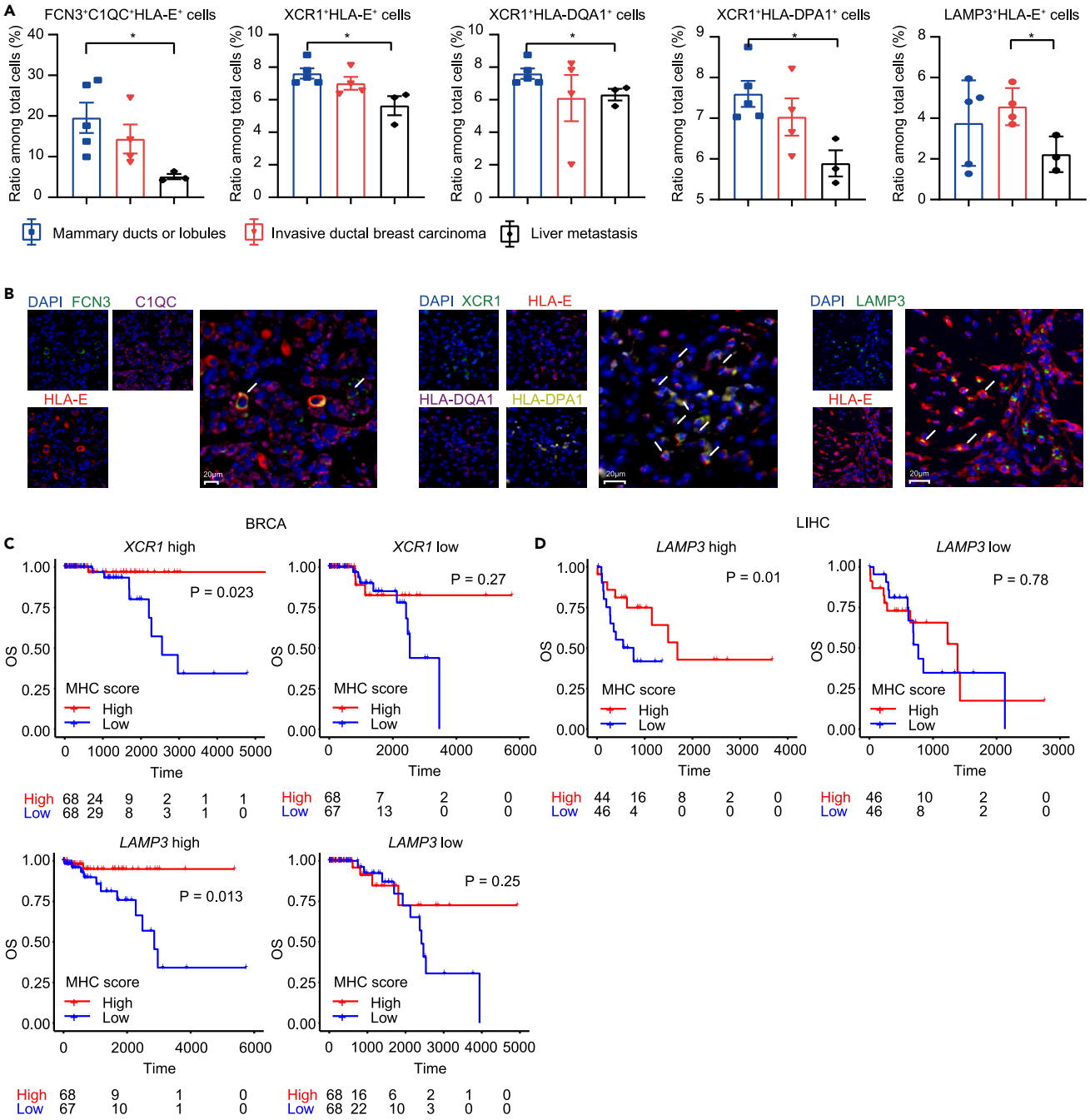

Figure 6. Clinical verification of alteration and function of FCN3$^+$ macrophage, cDC1 and LAMP3$^+$ DC in LM

(A) Ratio of FCN3$^+$C1QC$^+$HLA-E$^+$ cells, XCR1$^+$HLA-E$^+$ cells, XCR1$^+$HLA-DQA1$^+$ cells, XCR1$^+$HLA-DPA1$^+$ cells and LAMP3$^+$HLA-E$^+$ cells in normal mammary ducts or lobules, primary tumor of invasive ductal breast carcinoma (above phase 3C, staged by AJCC 6th Edition) and liver metastasis.

(B) Representative immunofluorescence appearance of FCN3$^+$C1QC$^+$HLA-E$^+$ cells, XCR1$^+$HLA-E$^+$ cells, XCR1$^+$HLA-DQA1$^+$ cells, XCR1$^+$HLA-DPA1$^+$ cells and LAMP3$^+$HLA-E$^+$ cells (above phase 3c, staged by AJCC 6th Edition). Panel 1 (left): blue for DAPI, green for FCN3, purple for C1QC and red for HLA-E; panel 2 (middle): blue for DAPI, green for XCR1, red for HLA-E, purple for HLA-DQA1 and yellow for HLA-DPA1; panel 3 (right): blue for DAPI, green for LAMP3 and red for HLA-E. Scale bar: 20 μm.

(C) Analysis of OS between patients with high and low levels of MHC signature score filtered by top and bottom 25% values of *XCR1* and *LAMP3* from the TCGA-BRCA cohort.

(D) Analysis of OS between patients with high and low levels of MHC signature score filtered by top and bottom 25% values of *LAMP3* from the TCGA-LIHC cohort.

In bar plots, Student's *t* test was performed. $p < 0.05$*, $p < 0.01$**, $p < 0.001$***, $p < 0.0001$****.

In survival analysis, Log rank was used to calculate the p value, $p < 0.05$ was considered to be significant.

and cause failure in killing the tumor cells migrated to the liver. The mechanism of macrophages affecting $CD4^+$ T cell infiltration and cDC1 regulating $CD8^+$ T cells by antigen presentation were also displayed in NPC-LM, THCA-LM and CESC-LM, indicating the general relevance.

Limitations of the study

Some limitations need to be acknowledged in this study. First, we only showed the changes of proportion among immune cells. We did not perform analysis of cell type proportions in whole tissue because there are much higher proportions of tumor cells in liver-metastasis than in adjacent tissues, which will profoundly affect the proportions of immune cells and lead to unconvincing results. Therefore, we removed tumor cells and other non-immune cells to re-compute the proportion of immune cells. Second, we manage to use the transcriptomic data of the TCGA BRCA and LIHC cohorts, which are bulk RNA-Seq, to analyze the influence of MHC expression in $FCN3^+$ macrophages, cDC1 and $LAMP3^+$ DC on overall survival. However, the markers of $FCN3^+$ macrophages, *FCN3* and *C1QC*, cannot separately represent this subtype of cells, we can not precisely divide the patients into groups by $FCN3^+$ macrophages enrichment.

STAR★METHODS

Detailed methods are provided in the online version of this paper and include the following:

- KEY RESOURCES TABLE
- RESOURCE AVAILABILITY
  - Lead contact
  - Materials availability
  - Data and code availability
- EXPERIMENTAL MODEL AND STUDY PARTICIPANT DETAILS
  - Ethics approval and consent to participate
  - Study participants
- METHOD DETAILS
  - Tissue dissociation and single-cell preparation
  - 10× library preparation and sequencing
  - scRNA-seq data processing and cell type identification
  - Analysis of functional pathway enrichment
  - Analysis of differentially expressed genes
  - Pseudo-time analysis
  - GSVA signature scoring
  - Cell-to-cell communication
  - Immunofluorescence
  - Survival analysis
  - Copy-number Karyotyping of Tumors
- QUANTIFICATION AND STATISTICAL ANALYSIS

SUPPLEMENTAL INFORMATION

Supplemental information can be found online at https://doi.org/10.1016/j.isci.2024.108896.

ACKNOWLEDGMENTS

We thank Shenglin Mei and Zhuang Wei for assistance in data analysis. This study was partially supported by grants from National Natural Science Foundation of China (81872895 and 82073881 to D.Z.; 81872915, 82073904 and 82011530150 to M.-W.W.), Shanghai Municipal Education Commission (Shanghai Top-Level University Capacity Building Program DGF817029-04 to M.-W.W.), Shanghai Science and Technology Commission (18ZR1403900, 20430713600 and 18JC1413800 to D.Z.) and Fudan-SIMM Joint Research Fund (FU-SIMM20181010 to D.Z. and D.Y.).

AUTHOR CONTRIBUTIONS

X.S.W., Y.Z., C.X. and W.Q.X. performed experimental studies; Q.T.Z., D.Y., W.Q.X. and L.W. analyzed the data; W.Z. conducted data curation, visualization and bioinformatics analysis with the supervision of D.Z; M.-W.W. secured funding, initiated and manage the project; D.Z. and M.-W.W. wrote the manuscript with assistance of W.Z., Y.Z. and X.S.W.

DECLARATION OF INTERESTS

The authors declare no competing interests.

Received: June 15, 2023
Revised: October 28, 2023
Accepted: January 9, 2024
Published: January 12, 2024

REFERENCES

1. Tsilimigras, D.I., Brodt, P., Clavien, P.-A., Muschel, R.J., D'Angelica, M.I., Endo, I., Parks, R.W., Doyle, M., de Santibañes, E., and Pawlik, T.M. (2021). Liver metastases. Nat. Rev. Dis. Prim. *7*, 27.
2. Tumeh, P.C., Rosenblum, M., Handley, N., Tsai, K., Rodriguez, R.R.S., Khurana, N., Harview, C., Spasic, M., Sanchez, P.J., Chang, J., et al. (2015). Metastatic site and response to pembrolizumab (anti-PD1 antibody) in melanoma. Cancer Res. *75*.
3. Topalian, S.L., Hodi, F.S., Brahmer, J.R., Gettinger, S.N., Smith, D.C., McDermott, D.F., Powderly, J.D., Sosman, J.A., Atkins, M.B., Leming, P.D., et al. (2019). Five-Year Survival and Correlates Among Patients With Advanced Melanoma, Renal Cell Carcinoma, or Non-Small Cell Lung Cancer Treated With Nivolumab. JAMA Oncol. *5*, 1411–1420.
4. Pires Da Silva, I., Lo, S., Quek, C., Gonzalez, M., Carlino, M.S., Long, G.V., and Menzies, A.M. (2020). Site-specific response patterns, pseudoprogression, and acquired resistance in patients with melanoma treated with ipilimumab combined with anti-PD-1 therapy. Cancer *126*, 86–97.
5. Yang, M., and Zhang, C. (2021). The role of liver sinusoidal endothelial cells in cancer liver metastasis. Am. J. Cancer Res. *11*, 1845–1860.
6. Shiraha, H., Iwamuro, M., and Okada, H. (2020). Hepatic Stellate Cells in Liver Tumor. Adv. Exp. Med. Biol. *1234*, 43–56.
7. Breous, E., Somanathan, S., Vandenberghe, L.H., and Wilson, J.M. (2009). Hepatic regulatory T cells and Kupffer cells are crucial mediators of systemic T cell tolerance to antigens targeting murine liver. Hepatology *50*, 612–621.
8. You, Q., Cheng, L., Kedl, R.M., and Ju, C. (2008). Mechanism of T cell tolerance induction by murine hepatic Kupffer cells. Hepatology *48*, 978–990.
9. Shetty, S., Lalor, P.F., and Adams, D.H. (2018). Liver sinusoidal endothelial cells - gatekeepers of hepatic immunity. Nat. Rev. Gastroenterol. Hepatol. *15*, 555–567.
10. Diehl, L., Schurich, A., Grochtmann, R., Hegenbarth, S., Chen, L., and Knolle, P.A. (2008). Tolerogenic maturation of liver sinusoidal endothelial cells promotes B7-homolog 1-dependent CD8+ T cell tolerance. Hepatology *47*, 296–305.
11. Yu, M.C., Chen, C.H., Liang, X., Wang, L., Gandhi, C.R., Fung, J.J., Lu, L., and Qian, S. (2004). Inhibition of T-cell responses by hepatic stellate cells via B7-H1-mediated T-cell apoptosis in mice. Hepatology *40*, 1312–1321.
12. Viñas, O., Bataller, R., Sancho-Bru, P., Ginès, P., Berenguer, C., Enrich, C., Nicolás, J.M., Ercilla, G., Gallart, T., Vives, J., et al. (2003). Human hepatic stellate cells show features of antigen-presenting cells and stimulate lymphocyte proliferation. Hepatology *38*, 919–929.
13. Bale, R., Putzer, D., and Schullian, P. (2019). Local Treatment of Breast Cancer Liver Metastasis. Cancers *11*, 1341.
14. De Kleer, I., Willems, F., Lambrecht, B., and Goriely, S. (2014). Ontogeny of myeloid cells. Front. Immunol. *5*, 423.
15. Etzerodt, A., and Moestrup, S.K. (2013). CD163 and inflammation: biological, diagnostic, and therapeutic aspects. Antioxidants Redox Signal. *18*, 2352–2363.
16. Nakamura, K., and Smyth, M.J. (2020). TREM2 marks tumor-associated macrophages. Signal Transduct. Targeted Ther. *5*, 233.
17. Ferris, S.T., Durai, V., Wu, R., Theisen, D.J., Ward, J.P., Bern, M.D., Davidson, J.T., 4th, Bagadia, P., Liu, T., Briseño, C.G., et al. (2020). cDC1 prime and are licensed by CD4(+) T cells to induce anti-tumour immunity. Nature *584*, 624–629.
18. Peng, Q., Qiu, X., Zhang, Z., Zhang, S., Zhang, Y., Liang, Y., Guo, J., Peng, H., Chen, M., Fu, Y.X., and Tang, H. (2020). PD-L1 on dendritic cells attenuates T cell activation and regulates response to immune checkpoint blockade. Nat. Commun. *11*, 4835.
19. Zhang, Q., He, Y., Luo, N., Patel, S.J., Han, Y., Gao, R., Modak, M., Carotta, S., Haslinger, C., Kind, D., et al. (2019). Landscape and Dynamics of Single Immune Cells in Hepatocellular Carcinoma. Cell *179*, 829–845.e20.
20. Dalod, M., Chelbi, R., Malissen, B., and Lawrence, T. (2014). Dendritic cell maturation: functional specialization through signaling specificity and transcriptional programming. EMBO J. *33*, 1104–1116.
21. Böttcher, J.P., and Reis e Sousa, C. (2018). The Role of Type 1 Conventional Dendritic Cells in Cancer Immunity. Trends Cancer *4*, 784–792.
22. Teicher, B.A., and Fricker, S.P. (2010). CXCL12 (SDF-1)/CXCR4 pathway in cancer. Clin. Cancer Res. *16*, 2927–2931.
23. Tokunaga, R., Zhang, W., Naseem, M., Puccini, A., Berger, M.D., Soni, S., McSkane, M., Baba, H., and Lenz, H.J. (2018). CXCL9, CXCL10, CXCL11/CXCR3 axis for immune activation - A target for novel cancer therapy. Cancer Treat Rev. *63*, 40–47.
24. Sánchez-Paulete, A.R., Cueto, F.J., Martínez-López, M., Labiano, S., Morales-Kastresana, A., Rodríguez-Ruiz, M.E., Jure-Kunkel, M., Azpilikueta, A., Aznar, M.A., Quetglas, J.I., et al. (2016). Cancer Immunotherapy with Immunomodulatory Anti-CD137 and Anti-PD-1 Monoclonal Antibodies Requires BATF3-Dependent Dendritic Cells. Cancer Discov. *6*, 71–79.
25. Böttcher, J.P., Bonavita, E., Chakravarty, P., Blees, H., Cabeza-Cabrerizo, M., Sammicheli, S., Rogers, N.C., Sahai, E., Zelenay, S., and Reis e Sousa, C. (2018). NK Cells Stimulate Recruitment of cDC1 into the Tumor Microenvironment Promoting Cancer Immune Control. Cell *172*, 1022–1037.e14.
26. Santagata, S., Napolitano, M., D'Alterio, C., Desicato, S., Maro, S.D., Marinelli, L., Fragale, A., Buoncervello, M., Persico, F., Gabriele, L., et al. (2017). Targeting CXCR4 reverts the suppressive activity of T-regulatory cells in renal cancer. Oncotarget *8*, 77110–77120.
27. Redjimi, N., Raffin, C., Raimbaud, I., Pignon, P., Matsuzaki, J., Odunsi, K., Valmori, D., and Ayyoub, M. (2012). CXCR3+ T regulatory cells selectively accumulate in human ovarian carcinomas to limit type I immunity. Cancer Res. *72*, 4351–4360.
28. Hafemeister, C., and Satija, R. (2019). Normalization and variance stabilization of single-cell RNA-seq data using regularized negative binomial regression. Genome Biol. *20*, 296.
29. Aran, D., Looney, A.P., Liu, L., Wu, E., Fong, V., Hsu, A., Chak, S., Naikawadi, R.P., Wolters, P.J., Abate, A.R., et al. (2019). Reference-based analysis of lung single-cell sequencing reveals a transitional profibrotic macrophage. Nat. Immunol. *20*, 163–172.
30. Wu, T., Hu, E., Xu, S., Chen, M., Guo, P., Dai, Z., Feng, T., Zhou, L., Tang, W., Zhan, L., et al. (2021). clusterProfiler 4.0: A universal enrichment tool for interpreting omics data. Innovation *2*, 100141.
31. Jin, S., Guerrero-Juarez, C.F., Zhang, L., Chang, I., Ramos, R., Kuan, C.H., Myung, P., Plikus, M.V., and Nie, Q. (2021). Inference and analysis of cell-cell communication using CellChat. Nat. Commun. *12*, 1088.
32. Gao, R., Bai, S., Henderson, Y.C., Lin, Y., Schalck, A., Yan, Y., Kumar, T., Hu, M., Sei, E., Davis, A., et al. (2021). Delineating copy number and clonal substructure in human tumors from single-cell transcriptomes. Nat. Biotechnol. *39*, 599–608.

STAR★METHODS

KEY RESOURCES TABLE

REAGENT or RESOURCE	SOURCE	IDENTIFIER
Antibodies		
Rabbit anti-FCN3 (C-term) Polyclonal Antibody	Absin	Cat# abs101543; RRID: AB_3083610
Rabbit anti-C1QC Polyclonal Antibody	Abclonal	Cat# A9227; RRID: AB_2768652
Mouse anti-HLA-E Monoclonal Antibody	Absin	Cat# abs154728; RRID: AB_3083609
Rabbit anti-XCR1 (D2F8T) Monoclonal Antibody	Cell Signaling Technology	Cat# 44665S; RRID: AB_3083608
Rabbit anti-HLA-DQA1 Polyclonal Antibody	Proteintech	Cat# 16918-1-AP; RRID: AB_2878332
Rabbit anti-HLA-DPA1 Polyclonal Antibody	Proteintech	Cat# 16109-1-AP; RRID: AB_1851387
Rabbit anti-LAMP3 Polyclonal Antibody	Abclonal	Cat# A2895; RRID: AB_2764715
Biological samples		
Human metastatic tumor in the liver and adjacent nonmalignant tissues	Fudan University Shanghai Cancer Center	https://www.shca.org.cn/
HBreD055CD01	Xinchao Biotechnology (Shanghai, China)	HBreD055CD01
Chemicals, peptides, and recombinant proteins		
MACS Tissues storage solution	Miltenyi Biotec	Cat# 130-100-008
Red Cell Lysis Buffer	Sigma-Aldrich	Cat# 11814389001
Qiagen Buffer EB	Qiagen	Cat# 19086
AO-PI stain	Logos biosystems	Cat# F23001
Bovine Serum Albumin	Sigma-Aldrich	Cat# A7030
Collagenase P	Roche	Cat# 11213865001
DNase I	Roche	Cat# 10104159001
Collagenase III	Sigma-Aldrich	Cat# 9007-34-5
Hyaluronidase	Sigma-Aldrich	Cat# 9001-54-1
Critical commercial assays		
Chromium Next GEM Single Cell 5' Kit v1.1	10× Genomics Chromium	Cat# PN-1000165
Single Index Kit T Set A, 96 rxns	10× Genomics Chromium	Cat# PN-1000213
Qubit™ dsDNA HS Assay Kit	Thermo Fisher Scientific	Cat# Q32854
Agilent High Sensitivity DNA Kit (D1000)	Agilent	Cat# 5067-5585
SPRIselect Reagent Kit	Beckman Coulter	Cat# B23318
Deposited data		
Single-cell RNA-seq data	This paper	GSE249361
Original code	This paper	https://doi.org/10.6084/m9.figshare.24827010.v1
Software and algorithms		
CaseViewer	3DHISTECH Ltd., Budapest, Hungary	2.4
Cellranger 6.0.2	10xGenomics	https://www.10xgenomics.com/support/software/cell-ranger
CellChat	http://www.cellchat.org/	1.4.0
clusterProfiler	clusterProfiler package in R	4.0.5
CopyKat	https://github.com/navinlabcode/copykat	1.0.8
GraphPad Prism	San Diego, GraphPad Software, USA	8
GSEA	www.gsea-msigdb.org	4.0.5

(*Continued on next page*)

Continued

REAGENT or RESOURCE	SOURCE	IDENTIFIER
GSVA	GSVA package in R	1.40.1
KEGG	http://www.genome.jp/kegg/	N/A
Monocle2 pipeline	Monocle2 package in R	2.20.0
PCA algorithm	R	1.2.5042
R	The R project for Statistical Computing	4.1.0
Seurat pipeline	Seurat package in R	4.0.6
UMAP	UMAP package in R	0.2.7.0
Other		
Chromium Single-Cell Platform	10× Genomics Chromium™	N/A
NovaSeq 6000 system instrument	Illumina	N/A
TCGA BRCA and LIHC cohorts	TCGA	GDC (https://portal.gdc.cancer.gov/)
Human reference genome NCBI build 38, GRCh38	Genome Reference Consortium	https://www.ncbi.nlm.nih.gov/grc/human
GO: Gene Ontology gene sets and KEGG subset of Canonical pathways	Molecular Signatures Database (MSigDB)	https://www.gsea-msigdb.org/gsea/msigdb/human/collections.jsp#H

RESOURCE AVAILABILITY

Lead contact

Further information and requests for resources and reagents should be directed to the lead contact, Dr. Ming-Wei Wang (mwwang@simm.ac.cn).

Materials availability

This study did not generate new unique reagents.

Data and code availability

- Single-cell RNA-seq data have been deposited at GEO and are publicly available as of the date of publication. Accession numbers are listed in the key resources table. This paper analyzes existing, publicly available data. These accession source for the datasets are listed in the key resources table.
- All original code has been deposited at FigShare and is publicly available as of the date of publication. DOIs are listed in the key resources table.
- Any additional information required to reanalyze the data reported in this paper is available from the lead contact upon request.

EXPERIMENTAL MODEL AND STUDY PARTICIPANT DETAILS

Ethics approval and consent to participate

The study protocols were approved by the Ethics Committee of Fudan University Shanghai Cancer Center (050432-4-1911D). Informed consent was signed by recruited patients. The clinical information of all patients is summarized in Table S1. The study was monitored by an independent data and safety monitoring board. Information on gender, ethnicity and socioeconomic status was not collected.

Study participants

In total 11 patients (females: n = 8: males: n = 3, between 33 and 62 years old, Table S1) volunteered to participate in this study, covering four tumor types with liver metastasis (6 breast cancer, 2 nasopharyngeal carcinoma, 2 thyroid carcinoma and 1 cervical cancer cases) from Fudan University Shanghai Cancer Center, were enrolled in this study and provided with informed consent. Following surgical resections, fresh specimens of the metastatic tumor in the liver and adjacent nonmalignant tissues (used as normal control) were processed for scRNA-seq analysis.

METHOD DETAILS

Tissue dissociation and single-cell preparation

Tissues were transported in MACS tissue storage solution (Miltenyi Biotec) on ice within 40 min to preserve viability. Samples were rinsed with ice-cold PBS, minced on ice to pieces of less than 1 mm^3 and then enzymatically dissociated for 15 min for metastatic liver tumor samples and 10 min for control liver samples at 37°C (with manual shaking every 5 min). Dissociation was carried out in DMEM containing 2 mg/mL collagenase P (Roche) and 0.2 mg/mL DNase I (Roche) as digestion medium for the tumor tissues. Collagenase III (1 mg/mL, Sigma-Aldrich) and

hyaluronidase (0.1 mg/mL, Sigma-Aldrich) were additionally introduced to the digestion medium containing metastatic cancer samples to increase cell viability. The digestion suspension was then filtered using a 40 μm nylon cell strainer (Falcon), followed by centrifugation at 300× *g* and 4°C for 5 min. The cell pellet was resuspended in red blood cell lysis buffer (Sigma-Aldrich) for 5 min at room temperature to remove red blood cells. Samples were centrifuged (250× *g*, 4°C, 5 min) and resuspended in 200–500 μL (estimated) PBS containing 0.4% BSA (Sigma-Aldrich) and filtered through 40 μm cell strainers. Finally, the concentration and viability of single-cell suspension were checked by a LUNA automated cell counter (Logos Biosystems), and the cells were diluted with PBS containing 0.04% BSA to about 700-1,200 cells/μL.

10× library preparation and sequencing

The single cells were loaded (aiming at 5,000 cells/sample for each chip position) onto and barcoded with a 10× Chromium Controller (10× Genomics) followed by library construction for scRNA-seq using the Chromium Single Cell 5′ Library and Gel Bead kit (V1.1) from 10× Genomics according to the manufacturer's instructions. The 5′ gene expression libraries were sequenced on a NovaSeq 6000 system (Illumina) until sufficient saturation was reached (77.03% on average). Fastq alignment was performed in Cellranger 6.0.2 with GRCh38 as transcriptome reference.

scRNA-seq data processing and cell type identification

To control the quality of scRNA-seq raw data of the tumor samples, Seurat (version 4.0.6) was used to routinely exclude single cells with <250 genes and <500 UMIs. Removal of batch effects among samples was realized with integration in Seurat. Sctransform[28] was performed to ensure normalization and variance stabilization of single-cell RNA-seq data, using sample site as variable for integration. Then, dimension reduction and visualization were done with principal component analysis (PCA) and uniform manifold approximation and projection (UMAP). Resolution is 0.5 and 30 PCs were used to run UMAP and clustering. For the sake of identifying major cell types, SingleR,[29] an automated cell labeling method, was performed based on data from Human Primary Cell Atlas. Specific marker genes of each cluster were found based on biological knowledge or the FindAllMarkers function in Seurat.

Analysis of functional pathway enrichment

To find altered pathways between LM and the adjacent tissue, GSEA (clusterProfiler,[30] version 4.0.5) was used to perform gene set enrichment analyses and all features (26,101 genes) in SCT assay were used. GO: Gene Ontology gene sets and KEGG subset of Canonical pathways were downloaded from the Molecular Signatures Database (MSigDB). Pathways with p value < 0.05 and involved in immunity were included for further analysis. Up-regulated and down-regulated pathways were visualized by barplots or enrichment curves.

To find which functional pathways works in different cells clusters, markers found with FindAllMarkers tool in Seurat was input for GO enrichment (clusterProfiler, version 4.0.5). Top 10 enriched pathways were visualized by bubble plots.

Analysis of differentially expressed genes

To explore the differentially expressed genes (DEGs) in each cluster during a dynamic development process, the FindMarkers tool from Seurat was used to calculate the number of DEGs. FindMarker Function was used with Wilcoxon Rank-Sum test as default to identify differentially expressed genes between two groups of cells. Adjusted p value was set at <0.05. The results were visualized by violin plots.

Pseudo-time analysis

The R package Monocle (version 2.20.0) was used to determine differentiation trajectories for $CD4^+$ T cells. Counts were input and differential genes were screened and used to reduce dimension by DDRTree method. Cell_trajectory was plotted and colored by sample location or gene expression of regulatory and exhausted markers.

GSVA signature scoring

MHC signature scores were calculated by gsva function with *Z* score method in Package GSVA (version 1.40.1). MHC signature: *HLA-A*, *HLA-B*, *HLA-C*, *HLA-DMA*, *HLA-DPA1*, *HLA-DPB1*, *HLA-DQA1*, *HLA-DQB1*, *HLA-DRA*, *HLA-DRB1* and *HLA-E*.

Cell-to-cell communication

To investigate the communication among cell clusters through ligands and receptors, CellChat[31] (R package, version 1.4.0) was applied to analyze intercellular crosstalk. A total of 29 clusters were explored for cell-cell networks. Data of LM and adjacent tissues were applied to CellChat respectively and interaction strengths (probability) were compared. Ligand–receptor pairs with p value of <0.05 were considered significant and their interaction strengths (probability) were of confidence.

Immunofluorescence

Immunofluorescence was performed on the tissue array, HBreD055CD01, purchased from Xinchao Biotechnology (Shanghai, China). Patient and sample information is displayed in Table S2. The sections were stained for three panels by using 4-color Novo-Light multiplex fluorescence immunohistochemistry: panel 1 including Rabbit anti-FCN3 (C-term) Polyclonal Antibody (abs101543, Absin), Rabbit anti-C1QC

Polyclonal Antibody (A9227, Abclonal) and Mouse anti-HLA-E Monoclonal Antibody (abs154728, Absin); panel 2 including Rabbit anti-XCR1 (D2F8T) Monoclonal Antibody (44665S, CST), Mouse anti-HLA-E Monoclonal Antibody (abs154728, Absin), Rabbit anti-HLA-DQA1 Polyclonal Antibody (16918-1-AP, Proteintech) and Rabbit anti-HLA-DPA1 Polyclonal Antibody (16109-1-AP, Proteintech); panel 3 including Rabbit anti-LAMP3 Polyclonal Antibody (A2895, Abclonal) and Mouse anti-HLA-E Monoclonal Antibody (abs154728, Absin). Briefly, the sections were incubated for 60 min with primary antibodies, and then incubated for 10 min with poly-HRP anti-mouse/rabbit IgG before incubation for 10 min with the corresponding fluorophores. Nuclei was stained with DAPI. After scanning the whole tissue arrays on the confocal laser scanning microscope, representative cells from the single-color slides were analyzed using CaseViewer software 2.4 (3DHISTECH Ltd., Budapest, Hungary). Sections of normal mammary ducts or lobules, primary tumor of invasive ductal breast carcinoma (above phase 3C, staged by AJCC 6th Edition) and liver metastasis from patients older than 35 years old were incorporated into following analysis.

Survival analysis

Survival analysis was performed in TCGA BRCA and LIHC cohorts and plotted on R. Data were downloaded in GDC (https://portal.gdc.cancer.gov/). OS was compared between patients with top 25% and bottom 25% levels of MHC signature scores. Respectively, survival analysis of MHC signature score was performed in patients with high and low expression of marker genes of target cells, extracted from top (high expression) and bottom (low expression) 25% values, respectively.

Copy-number Karyotyping of Tumors

Copy number variation was analyzed by Copy-number Karyotyping of Tumors (copykat,[32] version 1.0.8) to identify normal epithelial cells and tumor cells, with counts of RNA data input. Cells in the adjacent tissue were set as normal cells. Euclidean was chosen as the distance method. Other parameters and threshold are default.

QUANTIFICATION AND STATISTICAL ANALYSIS

Fastq alignment was performed in Cellranger 6.0.2. Single-cell RNA seq data and TCGA data were analyzed and plotted on R version 4.1.0. After immunofluorescence, representative cells from the single-color slides were analyzed using CaseViewer software 2.4 (3DHISTECH Ltd., Budapest, Hungary). When comparing proportion of cell types, paired t-test was performed, $p < 0.05$ was considered to be significant. In GSEA analysis results, the p values were adjusted by BM method, adjusted $p < 0.05$ was considered to be significant. In DE analysis, Wilcoxon Rank-Sum test was used to identify differentially expressed genes between two groups of cells. The p values that were used to graph had already been adjusted and adjusted $p < 0.05$ was considered to be significant. In gene expression analysis, paired t-test are performed. $p < 0.05$*, $p < 0.01$**, $p < 0.001$***, $p < 0.0001$****. Displaying ratio of FCN3$^+$C1QC$^+$HLA-E$^+$ cells, XCR1$^+$HLA-E$^+$ cells, XCR1$^+$HLA-DQA1$^+$ cells, XCR1$^+$HLA-DPA1$^+$ cells and LAMP3$^+$HLA-E$^+$ cells, Student's *t* test are performed. $p < 0.05$*, $p < 0.01$**, $p < 0.001$***, $p < 0.0001$****. In survival analysis, Log rank was used to calculate the p value, $p < 0.05$ was considered to be significant. All of the statistical details of experiments can be found in the figures and figure legends.